

Nonlinear robust observer based adaptive control design for variable speed wind turbine

Navdeep Singh*, Bhanu Pratap** and Akhilesh Swarup**

*School of Renewable Energy and Efficiency, National Institute of Technology Kurukshetra, India

**Electrical Engineering Department, National Institute of Technology Kurukshetra, India

**Corresponding Author: bhanumnit@gmail.com

ABSTRACT

This paper proposes a nonlinear robust observer based adaptive control of a three-bladed-horizontal-axis, variable speed wind turbine (VSWT). Due to irregular behavior of wind speed, the aerodynamic model of VSWT is considered as highly nonlinear and uncertain. As the rotor speed is the only measurable state, a sliding mode observer (SMO) is designed for the estimation of unmeasurable states. Also, a nonlinear friction and disturbance observer (NFDO) is employed to deal with the external disturbances and frictional effects across the shaft of the rotor and generator in VSWT system. On the basis of proposed observers (SMO and NFDO), an adaptive output feedback controller for VSWT is developed using quasi-sliding mode control technique. The proposed observer based controller is designed to capture maximum power available from the wind in the presence of uncertainties. The closed-loop stability of proposed observer based controller has been proven using Lyapunov-like design algorithm. The detailed simulation studies have been carried out to illustrate the robust performance of the proposed observer based control scheme. Finally, a comparative analysis of proposed adaptive controller with various controllers has been done to ensure the robust tracking performance with low chattering effect, lesser tracking errors, and bounded control efforts.

Keywords: Adaptive control; friction; quasi-sliding mode control; robust observer; variable speed wind turbine.

INTRODUCTION

The wind energy conversion system (WECS) contributes a large part of power production among various renewable energy sources such as solar, biomass, hydro, wind, and geothermal energy (Fan *et al.*, 2016; Njiri *et al.*, 2016). As per the report of Global Wind Energy Council (2016), power generation through wind has been increased about 8.3 GW (Douak *et al.*, 2018). There are several reasons behind the growing of wind Energy system such as emission free and low decommissioning cost of wind turbine (Singh *et al.*, 2016). The irregularity of wind speed due to randomly varying nature is a major problem in the control of variable speed wind turbine (VSWT). These irregularities of wind speed act as uncertainties for the VSWT in the attainment of maximum energy from the wind (Rezaei *et al.*, 2015). Due to these uncertainties, control system design of VSWT becomes essential for its smooth and efficient operations. The control design problem of the VSWT has received much attention over the past decade.

In literature, there are many significant contributions toward the control applications of VSWT. A proportional-integral-derivative (PID) controller is designed for torque control region of VSWT to achieve maximum power output from the wind by attaining the optimal tip speed ratio (Do *et al.*, 2018). Similarly, PID control is applied for the pitch control region of VSWT to maintain the power output constant by attaining rated rotor speed (Soued *et al.*, 2017). Correspondingly, a robust pitch controller based on H_∞ approach for VSWT is investigated in Moradi *et al.* (2015). The H_∞ control provides good results but it is not suitable for the system of higher order. An optimal controller based on linear quadratic regulator (LQR) for torque control of VSWT is reported for the tuning of optimum gain and bandwidth (Engleitner *et al.*, 2018). In the case of complex nonlinearities, uncertainties, and change in the operating

conditions, the performance of PID as well as LQR is restricted due to the requirement of adaptive tuning (Kamal *et al.*, 2013). Also, a model predictive control (MPC) based optimal control is illustrated for both torque and pitch control region of VSWT (Song *et al.*, 2017). This technique is effective, but very sensitive to cost weights functions optimization (Jain *et al.*, 2015). The quantitative feedback theory based robust controllers are investigated for the two-mass model of VSWT (Singh *et al.*, 2016; Singh *et al.*, 2017). However, these linear techniques are providing only local stability of the VSWT and may be unstable under unstructured perturbations and uncertainties.

VSWT is a highly nonlinear system, whereas the linear techniques may not provide satisfactory performance. Some of the nonlinear approaches applied to the VSWT control design are feedback linearization control (Toulabi *et al.*, 2017), sliding mode control (SMC) (Errami *et al.*, 2015), Backstepping control (Seker *et al.*, 2015), and intelligent controls based upon neuro-fuzzy (Asghar *et al.*, 2018) etc. A recursive design based approach, namely, backstepping controller applied on the VSWT, is reported by Seker *et al.*, 2015. To estimate effective wind speed, a neuro-fuzzy algorithm based intelligent controller for MPPT of VSWT has been demonstrated by Asghar *et al.*, 2018.

Sliding mode control is much popular in the literature among the robust control approaches (Mobayen *et al.*, 2016; Mobayen, 2016; Majd *et al.*, 2015). In SMC, the structure of closed-loop VSWT system is changed according to several decision rules called switching functions. The main features of the SMC are insensitive to the varying system parameters, uncertain disturbances, and a fast dynamical response, which abolishes the exact information about plant model (Mobayen, 2016). It is more suitable for the higher order nonlinear coupled dynamic VSWT system. In addition, if there is a small change in control efforts, it leads to high mechanical stress for the VSWT, which exhibits undesired chattering. To overcome the chattering problem, quasi-sliding mode control (QSMC) is one of the suitable approaches for the VSWT. The robust control design using QSMC has been investigated (Merida *et al.*, 2012; Merida *et al.*, 2014) for torque control of the two-bladed horizontal axis VSWT to achieve maximum power output where the power coefficients are too low (i.e., 0.3659 and 0.4291). Similarly, QSMC based controllers for pitch control of VSWT are reported by Xin *et al.*, 2014 and Zhang *et al.*, 2009. However, these controllers have successfully reduced the chattering and the mechanical stress acting on the VSWT (Pratap *et al.*, 2018b).

All the aforementioned nonlinear controllers are designed on the basis of exact information of actual/estimated state variables for the proper monitoring of the process, fault detection, and robust performance. Usually, all the state variables of the VSWT are not available for the measurements, which are required for the control design. Thus, the observer design for the VSWT is one of the better solutions (Shaik *et al.*, 2011; Pratap *et al.*, 2013). In the literature, various types of observers are presented for the VSWT. The aerodynamic torque has been estimated using sliding mode observer (SMO) designed for VSWT (Ciccarelli *et al.*, 2012; Corradini *et al.*, 2013). To estimate the stator flux linkage and rotor position of VSWT a quasi-sliding mode observer (QSMO) has been deliberated with a low range of sampling frequency (Zhang *et al.*, 2012b). Similarly, an SMO is investigated by Yang *et al.*, 2015, which estimates the rotor position and electromagnetic torque of the VSWT model.

In the presence of system nonlinearity, uncertain disturbances, effect of friction, the control system moves towards the unstable condition (Mobayen, 2015). A perturbation observer has been designed (Ren *et al.*, 2016) to estimate unknown disturbance for the two-mass model of VSWT to compensate the unknown dynamics of VSWT. The unknown wind speed and aerodynamic torque of a wind turbine have been estimated by Do *et al.*, 2017, through a nonlinear disturbance observer. However, these papers focused on the estimation of disturbances, without considering the effect of relative wind speed and the effect of frictions on the wind turbine.

In the literature, there are very few contributions of the observer based control design for the VSWT nonlinear model. The aerodynamic torque observer based robust controllers for VSWT model using the sliding mode approach have been reported by Ciccarelli *et al.*, 2012; Corradini *et al.*, 2013. A Backstepping controller is designed using high gain observer (Zhang *et al.*, 2012a) for wind turbine. Galeazzi *et al.*, 2013 have investigated a reduced order observer based output feedback Backstepping controller for the two-mass model of the VSWT. A nonlinear observer based model predictive controller for speed sensorless induction generator wind turbine systems is investigated (Merabet *et al.*, 2012). Also, a model reference adaptive controller is designed for WECS using Backstepping approach (Zu *et al.*

al., 2012). In the above studies, most of the papers focused only on the torque control of VSWT. The observer based control design problem for both torque and pitch control of VSWT has not received much attention.

In this paper, the torque and pitch control design of VSWT has been attempted to address the issues of stability, improved performance, robustness in presence of uncertainties, unavailability of states for feedback, and extraction of maximum power. A comprehensive model of VSWT is considered here, which includes three bladed horizontal axis structures. The proposed scheme implements the estimation of (i) VSWT states using sliding mode observer (SMO), and (ii) uncertainties using nonlinear friction and disturbance observer (NFDO). The estimated information is then used to design an adaptive control based on quasi-sliding mode technique. The bounds of uncertainties and the stability have been incorporated in the design using Lyapunov approach. The controller gains are made adaptive by implementation of a radial basis function neural network (RBFNN). Thus, the proposed work is a novel contribution among the robust observer based adaptive controller design for VSWT with a broad range of specifications such as states estimation, friction and disturbance approximation and its compensation, reference tracking, error reduction, fast convergence, and input constraints. Finally, the performance analysis of the designed controller has been done using simulation studies. The simulation results have been compared with the standard wind turbine controller (SWTC), proportional-integral (PI) controller, quantitative feedback theory (QFT) based controller, etc. to show the applicability of the proposed controller.

PRELIMINARIES

Mechanical modeling of VSWT

The work of VSWT depends on the varying nature of wind speed. The VSWT mechanical model is made up of various models, namely, aero-dynamics, rotor mechanics, tower dynamics, generator, and pitch actuation (Henriksen, 2007). The VSWT blades on the rotor side transform the wind kinetic energy into the mechanical energy by providing the aerodynamic torque and thrust force with the rotor effective wind speed.

Aerodynamic Model: The transformation of mechanical energy from wind kinetic energy is held by effectively providing the aerodynamic torque T_r given by

$$T_r = \frac{P_r}{\omega_r} \quad (1)$$

where ω_r = rotor speed; P_r = equivalent power generation during the interaction of turbine blades with wind being given by the following relation:

$$P_r = \frac{1}{2} \rho \pi R^2 v_w^3 C_p(\lambda, \theta) \quad (2)$$

where ρ = air density, R = radius of the wing, v_w = wind speed, and $C_p(\lambda, \theta)$ = coefficient of power performance, which is defined as (Dahbi *et al.*, 2016; Soufi *et al.*, 2016)

$$C_p(\lambda, \theta) = \{0.5 - 0.0167(\theta - 2)\} \sin \left\{ \frac{\pi(\lambda + 0.1)}{18 - 0.3(\theta - 2)} \right\} - 0.00184(\lambda - 3)(\theta - 2) \quad (3)$$

where θ = blade pitch angle, and λ = tip speed ratio given as

$$\lambda = \frac{\omega_r R}{v_w^r} \quad (4)$$

where v_w^r = relative wind speed.

A thrust force F_t on the rotor and turbine is also exerted by the wind given as

$$F_t = \frac{1}{2} \rho \pi R^2 v_w^2 C_t(\lambda, \theta) \quad (5)$$

where $C_t(\lambda, \theta)$ = coefficient of thrust, which is defined as

$$C_t(\lambda, \theta) = \frac{C_p(\lambda, \theta)}{\lambda}. \quad (6)$$

where C_p and C_t are typically known from the measurements or can be provided by wind turbine blade manufacturers (Jain *et al.*, 2015).

Rotor Mechanics Model: The wind turbine is separated from the transmission as rotor side and generator side. The rotor side inertia (J_r) and generator side inertia (J_g) are represented by the leftmost and rightmost disc, respectively, as reported in Fig. 1 (Thomsen, 2006).

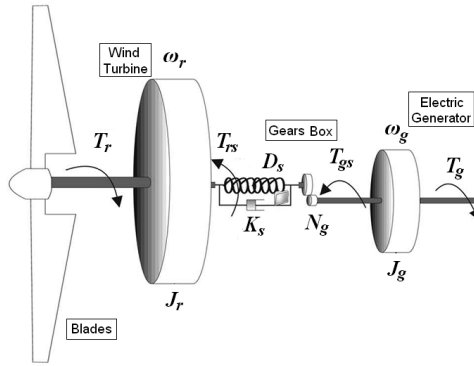


Fig. 1. Schematic of the variable speed wind turbine mechanics (Thomsen, 2006).

The dynamic nature of the shaft is described by the damping coefficient D_s and the spring constant K_s . On the left side, the model is excited by the rotor torque T_r and on the right side, the generator torque T_g . The torques at each side of the transmission (T_{rs} and T_{gs}) are related by the gear ratio,

$$T_{gs} = \frac{T_{rs}}{N_g} \quad (7)$$

where N_g is the gear ratio illustrated by the discs in the middle. According to the Newton second law of mechanics, the equations for the rotor and generator sides are illustrated as

$$\dot{\omega}_r J_r = T_r - T_{rs} \quad (8)$$

$$\dot{\omega}_g J_g = T_{gs} - T_g \quad (9)$$

The governing equations for describing the twist of the flexible shaft are as follows:

$$T_{rs} = D_s \dot{\delta} + K_s \delta \quad (10)$$

$$\delta = \Omega_r - \frac{\Omega_g}{N_g} \quad (11)$$

$$\dot{\delta} = \omega_r - \frac{\omega_g}{N_g} \quad (12)$$

where δ = twist of rotor shaft, Ω_r = angular position of the rotor shaft, Ω_g = angular position of the generator shaft, ω_r = angular velocity of the rotor shaft and ω_g = angular velocity of the generator shaft.

Tower Dynamics Model: The tower exhibits fore and aft motion due to the variability of the thrust force F_t , whose displacement ξ is modeled by assuming a spring-mass-damper system.

$$M_t \ddot{\xi} + D_t \dot{\xi} + K_t \xi = F_t \quad (13)$$

where $\dot{\xi}$ = velocity of tower, M_t = mass constant, D_t = damping constant and K_t = spring constant of the tower respectively. The relative wind speed v_w^r at the rotor is changed by movement of the tower given by

$$v_w^r = v_w - \dot{\xi} \quad (14)$$

Generator Dynamics Model: The Generator is modeled as a first order system with time constant τ_T .

$$\dot{T}_g = -\frac{1}{\tau_T} T_g + \frac{1}{\tau_T} T_{g,ref} \quad (15)$$

where $T_{g,ref}$ = demanded torque and T_g = the output torque. Assume that the losses in the transmission are zero. Therefore, the power output P_e is given by

$$P_e = T_g \omega_g \quad (16)$$

Pitch Actuation Model: The blade pitch is changed by a mechanical/hydraulic actuator assumed to follow the second order system dynamics,

$$\ddot{\theta} + 2\zeta\omega_n \dot{\theta} + \omega_n^2 \theta = \omega_n^2 \theta_{ref} \quad (17)$$

where θ_{ref} = demanded pitch angles, θ = actual pitch angles, ζ = damping of pitch actuator and ω_n = natural frequency of the actuator. The VSWT system parameters (Jain *et al.*, 2015) for the simulation study are presented in Table A1 (Refer Appendix). The block diagram of the overall dynamics of VSWT nonlinear model is depicted in Fig. 2.

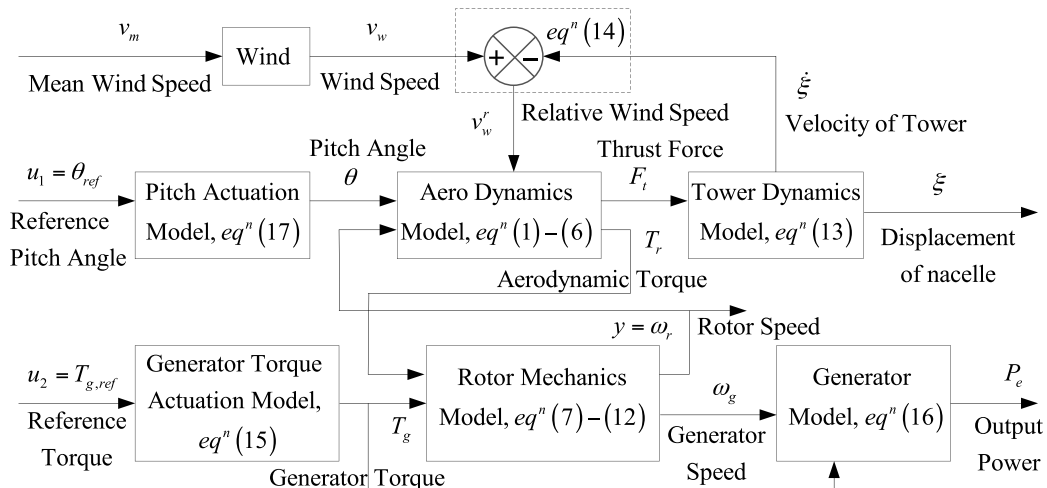


Fig. 2. Interconnected sub-models of VSWT relating the dynamical characteristics (Singh *et al.*, 2018).

The complete dynamics of the VSWT model (1)-(17) can be expressed in the form of differential equations as

$$\frac{d}{dt} \omega_r = \frac{1}{J_r} \frac{P_r(\omega_r, \theta, v_w^r)}{\omega_r} - \frac{D_s}{J_r} \omega_r + \frac{D_s}{J_r N_g} \omega_g - \frac{K_s}{J_r} \delta - \frac{1}{J_r} F_r(\omega_r) \quad (18a)$$

$$\frac{d}{dt} \omega_g = \frac{D_s}{J_g N_g} \omega_r - \frac{D_s}{J_g N_g^2} \omega_g + \frac{K_s}{J_g N_g} \delta - \frac{T_g}{J_g} - \frac{1}{J_g} F_g(\omega_g) \quad (18b)$$

$$\frac{d}{dt} \delta = \omega_r - \frac{1}{N_g} \omega_g \quad (18c)$$

$$\frac{d}{dt} \xi = \dot{\xi} \quad (18d)$$

$$\frac{d}{dt} \dot{\xi} = -\frac{K_t}{M_t} \xi - \frac{D_t}{M_t} \dot{\xi} + \frac{1}{M_t} F_t(\omega_r, \theta, v_w^r) \quad (18e)$$

$$\frac{d}{dt} \theta = \dot{\theta} \quad (18f)$$

$$\frac{d}{dt} \dot{\theta} = -\omega_n^2 \theta - 2\zeta \omega_n \dot{\theta} + \omega_n^2 \theta_{ref} \quad (18g)$$

$$\frac{d}{dt} T_g = -\frac{1}{\tau_T} T_g + \frac{1}{\tau_T} T_{g,ref} \quad (18h)$$

Nonlinear friction modeling of VSWT

Due to the heavier structure of VSWT, the components used for wind turbine are more flexible and deformable. VSWT components are often subjected to the problems of damages caused by frictions. The damage can drastically reduce the VSWT component's expected lifetime and is very expensive to repair. The availability of frictions in VSWT produces several effects such as stiction effect, viscous friction effect, and coulomb friction effect (Stevanovic *et al.*, 2016; Viveiros *et al.*, 2015). A highly nonlinear and complex friction model is added to increase the accuracy of VSWT model, which is composed of coulomb, viscous, and static friction terms. The friction model F_r and F_g across the rotor shaft and generator shaft are described as (De Wit *et al.*, 1995)

$$F_r = F_c \operatorname{sgn}(\omega_r) + (F_s - F_c) e^{-(\omega_r/v_s)^2} \operatorname{sgn}(\omega_r) + F_v \omega_r \quad (19a)$$

$$F_g = F_c \operatorname{sgn}(\omega_g) + (F_s - F_c) e^{-(\omega_g/v_s)^2} \operatorname{sgn}(\omega_g) + F_v \omega_g \quad (19b)$$

where F_c is the coulomb friction, F_s is the stiction friction, F_v is the viscous friction, and V_s is the stiction velocity. Incorporating a nonlinear friction to the VSWT model ensures the enhancement of the complexity of the system, but it provides a more precise dynamical model of the VSWT system. These frictions along with external disturbances are estimated using NFDO in the section nonlinear friction and disturbance observer design. In the next section, RBFNN structure has been introduced.

Structure of radial basis function neural network (RBFNN)

The proposed adaptive controller for VSWT has been designed using RBFNN. The RBFNN is an efficient, intelligent tool for the approximation of arbitrary input-output mappings, which can produce nonlinear decision boundaries (Jafarnejadsani *et al.*, 2013). The RBFNN consists of three layers, that is, input, hidden, and output layers as shown in Fig. 3.

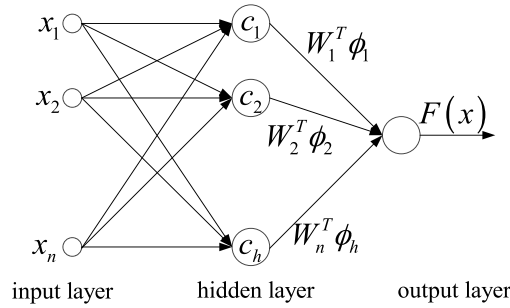


Fig. 3. The structure of a radial basis function neural network (Jafarnejadsani *et al.*, 2013).

The hidden units (radial centers) present a set of functions that comprise an arbitrary basis for the input patterns. The radial centers are represented by the vector $C_i, i=1, \dots, h$, where h is the number of radial centers in the hidden layer. The inputs are clustered around the centers and the output is linear in terms of RBFNN weights W_i .

$$F(x) = \sum_{i=1}^h W_i^T \phi_i \tag{20}$$

where $\phi_i = \phi(\|x - c_i\|)$ is the radial basis function and $\|x - c_i\|$ is the Euclidean distance between x and c_i . A common choice of radial basis function (RBF) is defined as

$$\phi(\|x - c_i\|) = e^{-\frac{\|x - c_i\|^2}{2\psi_i^2}} \tag{21}$$

The above expression is known as Gaussian RBF. The weights of the RBFNN can be tuned online using the weight adaptation law.

Problem Formulation

The nonlinear VSWT model (18) is described in the state space form as follows:

$$\begin{aligned} \dot{x} &= f(x, v_w^r) + gu + F_N(x) + d \\ y &= h(x) \end{aligned} \tag{22}$$

where $x = [\omega_r \ \omega_g \ \delta \ \xi \ \dot{\xi} \ \theta \ \dot{\theta} \ T_g]^T = [x_1 \ x_2 \ x_3 \ x_4 \ x_5 \ x_6 \ x_7 \ x_8]^T$ = state vector, $u = [\theta_{ref} \ T_{g,ref}]^T = [u_1 \ u_2]^T$ = input vector, $y = \omega_r = x_1$ = output vector and the matrices

$$f(x, v_w^r) = \begin{bmatrix} \bar{f}_1(x) + A_{11}x_1 + A_{12}x_2 + A_{13}x_3 \\ A_{21}x_1 + A_{22}x_2 + A_{23}x_3 + A_{28}x_8 \\ x_1 + A_{32}x_2 \\ x_5 \\ A_{54}x_4 + A_{55}x_5 + \bar{f}_5(x) \\ x_7 \\ A_{76}x_6 + A_{77}x_7 \\ A_{88}x_8 \end{bmatrix} \equiv \begin{bmatrix} f_1(x) \\ f_2(x) \\ f_3(x) \\ f_4(x) \\ f_5(x) \\ f_6(x) \\ f_7(x) \\ f_8(x) \end{bmatrix}; \quad g = \begin{bmatrix} 0 & 0 \\ 0 & 0 \\ 0 & 0 \\ 0 & 0 \\ 0 & 0 \\ 0 & 0 \\ g_7 & 0 \\ 0 & g_8 \end{bmatrix}; \quad h(x) = x_1 \quad \text{with the constants}$$

$$\bar{f}_1(x) = \frac{P_r(\omega_r, \theta, v_w^r)}{J_r} \frac{1}{\omega_r}; \quad A_{11} = \frac{-D_s}{J_r}; \quad A_{12} = \frac{D_s}{J_r N_g}; \quad A_{13} = \frac{-K_s}{J_r}; \quad A_{21} = \frac{D_s}{J_g N_g}; \quad A_{22} = \frac{-D_s}{J_g N_g^2}; \quad A_{23} = \frac{K_s}{J_g N_g};$$

$$A_{28} = \frac{-1}{J_g}; \quad A_{32} = \frac{-1}{N_g}; \quad A_{54} = \frac{-K_t}{M_t}; \quad A_{55} = \frac{-D_t}{M_t}; \quad \bar{f}_5(x) = \frac{F_t(\omega_r, \theta, v_w^r)}{M_t}; \quad A_{76} = -\omega_n^2; \quad A_{77} = -2\xi\omega_n;$$

$A_{88} = -\frac{1}{\tau_T}; \quad g_7 = \omega_n^2; \quad g_8 = \frac{1}{\tau_T}; \quad F_N(x) = \begin{bmatrix} -F_r(x) & -F_g(x) & 0 & 0 & 0 & 0 & 0 & 0 \end{bmatrix}^T$ = friction term considered in the plant and $d = [d_1 \ d_2 \ d_3 \ d_4 \ d_5 \ d_6 \ d_7 \ d_8]^T$ = time-varying external disturbances which are bounded.

Operating Regions of VSWT: The VSWT generally operates in four regions due to varying wind speeds as shown in Fig. 4 (Jafarnejadsani *et al.*, 2013; Merida *et al.*, 2014).

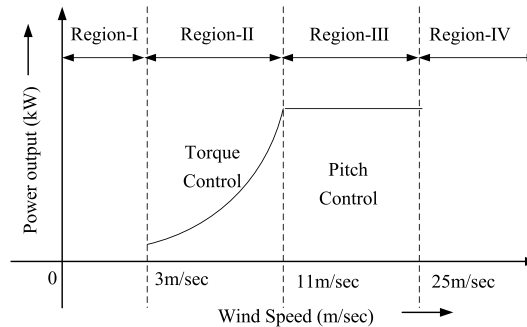


Fig. 4. Regions of operation for the VSWT at different wind speed (Jafarnejadsani *et al.*, 2013; Merida *et al.*, 2014).

In Region I: There is no power generation (wind speed is lower than the cut-in wind speed).

In Region II: The maximum power output is extraction (wind speeds lie between cut-in and rated wind speed).

In Region III: The constant power is maintained, which was obtained in Region II (wind speeds lie between rated and cut-out wind speed).

In Region IV: The VSWT remains shut-down (wind speeds beyond the cut-out wind speed).

The objective of this paper is to develop an adaptive controller for torque and pitch control of VSWT in Region II and Region III, respectively.

Torque Control Region (TCR): In this region, the reference pitch angle (θ_{ref}) remains fixed at zero and the reference

generator torque $T_{g,ref}$ is used as control input, which forces the measured rotor speed (ω_r) to track optimal rotor speed ($\omega_{r,opt}$). Thus, the VSWT operates in TCR between cut-in and rated wind speed to capture maximum power from the wind where the optimal tip-speed ratio λ_{opt} can be obtained as (Jafarnejadsani *et al.*, 2013)

$$\lambda_{opt} = \frac{\omega_{r,opt} R}{v_w} \quad (23)$$

which leads to a maximum point $C_{p,max} = C_p(\lambda_{opt}, \theta_{opt})$ for the production of maximum power. For the considered wind turbine, the $\lambda - C_p$ characteristic has been obtained as shown in Fig. 5.

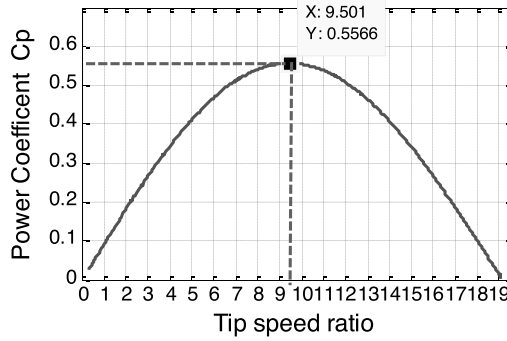


Fig. 5. Tip speed ratio λ Vs. Power Coefficient C_p curve.

From the above characteristic, the λ_{opt} is obtained as 9.5 at $C_{p,max} = 0.55$. Thus, the optimal rotor speed $\omega_{r,opt}$ can be determined using (23) as

$$\omega_{r,opt} = \frac{\lambda_{opt} v_w}{R} \quad (24)$$

Therefore, the proposed control scheme would regulate the measured rotor speed (ω_r) at an optimal rotor speed $\omega_{r,opt}$ with tip-speed ratio λ_{opt} .

Pitch Control Region (PCR): In this region, the reference generator torque ($T_{g,ref}$) remains fixed at its rated value and the reference pitch angle (θ_{ref}) is used as control input, which forces the measured rotor speed (ω_r) to regulate at the rated rotor speed ($\omega_{r,rated}$). Thus, the VSWT operates in PCR between the rated and cut-out wind speed to maintain the constant power from the wind. The rated/nominal value of reference generator torque is calculated as $T_{g,ref(nominal)} = P_{e,nom} / \omega_{g,nom}$, where $P_{e,nom}$ is the nominal power capacity of the wind turbine and $\omega_{g,nom}$ is the nominal angular velocity of generator (Jafarnejadsani *et al.*, 2013).

The control objectives of this paper are to design and implement:

- (i) an SMO, where observer states \hat{x}_i converge to the plant states x_i i.e., $\lim_{t \rightarrow \infty} (x_i - \hat{x}_i) = 0$, where $i = 1, \dots, 8$.
- (ii) an NFDO, which estimates the unknown frictions and external disturbances of the plant.
- (iii) an observer based adaptive controller, where the plant output $y = \omega_r$ tracks a specified smooth reference trajectory $y_d = \omega_{r,opt}$ in TCR and $y_d = \omega_{r,rated}$ in PCR i.e. $\lim_{t \rightarrow \infty} (y - y_d) = 0$.

The proposed robust observers and observer based controller are designed in the next sections.

SLIDING MODE OBSERVER (SMO) DESIGN

In the SMO, the estimation errors between plant and observer are fed back via a discontinuous switching signal instead of feeding it back linearly. It has an exclusive quality of generating sliding mode on the estimation errors. It is also well recognized that SMOs explicitly account for the modeling errors of plant. The robust nonlinear observer for VSWT model (22) is given as

$$\begin{aligned}\dot{\hat{x}} &= \hat{f}(\hat{x}, v_w^r) + gu + \alpha\sigma_1 + K \operatorname{sgn}(\sigma_1) \\ \hat{y} &= h(\hat{x})\end{aligned}\quad (25)$$

where $\hat{x} = [\hat{x}_1 \ \hat{x}_2 \ \hat{x}_3 \ \hat{x}_4 \ \hat{x}_5 \ \hat{x}_6 \ \hat{x}_7 \ \hat{x}_8]^T$ is estimate of plant state vector x , $\sigma_1 = x_1 - \hat{x}_1$ is the rotor speed estimation error, and the gains of the SMO are $\alpha = [\alpha_1 \ \alpha_2 \ \alpha_3 \ \alpha_4 \ \alpha_5 \ \alpha_6 \ \alpha_7 \ \alpha_8]^T$ and $K = [K_1 \ K_2 \ K_3 \ K_4 \ K_5 \ K_6 \ K_7 \ K_8]^T$.

Let $\sigma = x - \hat{x}$ be the estimation error of the states of VSWT. The time-derivative of σ can be obtained by subtracting (25) from (22),

$$\dot{\sigma} = \tilde{f}(x, \hat{x}, v_w^r) + T_{Fd} - \alpha\sigma_1 - K \operatorname{sgn}(\sigma_1)\quad (26)$$

where $\tilde{f}(x, \hat{x}, v_w^r) = f(x, v_w^r) - \hat{f}(\hat{x}, v_w^r) \equiv A\sigma + \tilde{\tilde{f}}(x, \hat{x}, v_w^r)$ and $T_{Fd}(x, t) \in \mathfrak{R}^8 = F_N(x) + d$ is considered as unknown uncertainty. Matrix A and vector $\tilde{\tilde{f}}(x, \hat{x}, v_w^r)$ are given by

$$A = \begin{bmatrix} A_{11} & A_{12} & A_{13} & 0 & 0 & 0 & 0 & 0 \\ A_{21} & A_{22} & A_{23} & 0 & 0 & 0 & 0 & A_{28} \\ 1 & A_{32} & 0 & 0 & 0 & 0 & 0 & 0 \\ 0 & 0 & 0 & 0 & 1 & 0 & 0 & 0 \\ 0 & 0 & 0 & A_{54} & A_{55} & 0 & 0 & 0 \\ 0 & 0 & 0 & 0 & 0 & 0 & 1 & 0 \\ 0 & 0 & 0 & 0 & 0 & A_{76} & A_{77} & 0 \\ 0 & 0 & 0 & 0 & 0 & 0 & 0 & A_{88} \end{bmatrix} \quad \text{and} \quad \tilde{\tilde{f}}(x, \hat{x}, v_w^r) = \begin{bmatrix} \tilde{\tilde{f}}_1(x) \\ 0 \\ 0 \\ 0 \\ \tilde{\tilde{f}}_5(x) \\ 0 \\ 0 \\ 0 \end{bmatrix}.$$

where $\tilde{\tilde{f}}_1(x) = \bar{f}_1(x) - \hat{f}_1(\hat{x})$ and $\tilde{\tilde{f}}_5(x) = \bar{f}_5(x) - \hat{f}_5(\hat{x})$.

Simplifying (26) gives

$$\dot{\sigma} = A_0\sigma + \tilde{\tilde{f}}(x, \hat{x}, v_w^r, t) - K \operatorname{sgn}(\sigma_1)\quad (27)$$

$$\text{where} \quad A_0 = \begin{bmatrix} A_{11} - \alpha_1 & A_{12} & A_{13} & 0 & 0 & 0 & 0 & 0 \\ A_{21} - \alpha_2 & A_{22} & A_{23} & 0 & 0 & 0 & 0 & A_{28} \\ 1 - \alpha_3 & A_{32} & 0 & 0 & 0 & 0 & 0 & 0 \\ -\alpha_4 & 0 & 0 & 0 & 1 & 0 & 0 & 0 \\ -\alpha_5 & 0 & 0 & A_{54} & A_{55} & 0 & 0 & 0 \\ -\alpha_6 & 0 & 0 & 0 & 0 & 0 & 1 & 0 \\ -\alpha_7 & 0 & 0 & 0 & 0 & A_{76} & A_{77} & 0 \\ -\alpha_8 & 0 & 0 & 0 & 0 & 0 & 0 & A_{88} \end{bmatrix}, \quad \tilde{\tilde{f}}(x, \hat{x}, v_w^r, t) = \begin{bmatrix} \tilde{\tilde{f}}_1(x) + T_{Fd_1} \\ T_{Fd_2} \\ T_{Fd_3} \\ T_{Fd_4} \\ \tilde{\tilde{f}}_5(x) + T_{Fd_5} \\ T_{Fd_6} \\ T_{Fd_7} \\ T_{Fd_8} \end{bmatrix},$$

and the positive constants α_i ($i=1..8$) are chosen in such a way that the eigen-values of matrix A_0 are at the desired position in the left-half of the s-plane. The rotor speed estimation error dynamics can be obtained as the first row of (27) as

$$\dot{\sigma}_1 = (A_{11} - \alpha_1)\sigma_1 + A_{12}\sigma_2 + A_{13}\sigma_3 + \tilde{f}_1(x, \hat{x}, v_w', t) - K_1 \text{sgn}(\sigma_1) \tag{28}$$

The observer gain K_1 is chosen sufficiently large to ensure sliding $\sigma_1 \dot{\sigma}_1 \leq 0$, (Laghrouche *et al.*, 2014), i.e.,

$$\sigma_1 \left\{ (A_{11} - \alpha_1)\sigma_1 + A_{12}\sigma_2 + A_{13}\sigma_3 + \tilde{f}_1(x, \hat{x}, v_w', t) - K_1 \text{sgn}(\sigma_1) \right\} \leq 0 \tag{29}$$

The state estimation error σ_1 would converge to the switching surface in the finite time (i.e. $\sigma_1 = 0$). Using an equivalent control algorithm (Laghrouche *et al.*, 2014), the following equation is obtained as

$$K_1 \text{sgn}(\sigma_1) \geq A_{12}\sigma_2 + A_{13}\sigma_3 + \tilde{f}_1(x, \hat{x}, v_w', t) \tag{30}$$

or
$$\text{sgn}(\sigma_1) = K_1^{-1} \left(A_{12}\sigma_2 + A_{13}\sigma_3 + \tilde{f}_1(x, \hat{x}, v_w', t) \right) \tag{31}$$

Now, define $\bar{\sigma} = [\sigma_2 \ \sigma_3 \ \sigma_4 \ \sigma_5 \ \sigma_6 \ \sigma_7 \ \sigma_8]^T$. Substituting (31) in (27) results in

$$\dot{\bar{\sigma}} = \bar{A}\bar{\sigma} + \bar{\delta} \tag{32}$$

where $\bar{\delta} = \delta + \tilde{f}(x, \hat{x}, v_w', t)$. Matrix \bar{A} and nonlinear function δ are given by

$$\bar{A} = \begin{bmatrix} (A_{22} - K_2 K_1^{-1} A_{12}) & (A_{23} - K_2 K_1^{-1} A_{13}) & 0 & 0 & 0 & 0 & A_{28} \\ (A_{32} - K_3 K_1^{-1} A_{12}) & -K_3 K_1^{-1} A_{13} & 0 & 0 & 0 & 0 & 0 \\ -K_4 K_1^{-1} A_{12} & -K_4 K_1^{-1} A_{13} & 0 & 1 & 0 & 0 & 0 \\ -K_5 K_1^{-1} A_{12} & -K_5 K_1^{-1} A_{13} & A_{54} & A_{55} & 0 & 0 & 0 \\ -K_6 K_1^{-1} A_{12} & -K_6 K_1^{-1} A_{13} & 0 & 0 & 0 & 1 & 0 \\ -K_7 K_1^{-1} A_{12} & -K_7 K_1^{-1} A_{13} & 0 & 0 & A_{76} & A_{77} & 0 \\ -K_8 K_1^{-1} A_{12} & -K_8 K_1^{-1} A_{13} & 0 & 0 & 0 & 0 & A_{88} \end{bmatrix} \text{ and } \delta = \begin{bmatrix} -K_2 K_1^{-1} \tilde{f}_1(x) \\ -K_3 K_1^{-1} \tilde{f}_1(x) \\ -K_4 K_1^{-1} \tilde{f}_1(x) \\ -K_5 K_1^{-1} \tilde{f}_1(x) \\ -K_6 K_1^{-1} \tilde{f}_1(x) \\ -K_7 K_1^{-1} \tilde{f}_1(x) \\ -K_8 K_1^{-1} \tilde{f}_1(x) \end{bmatrix} .$$

The observer gains K_i ($i=1..8$) are selected in such a way that matrix \bar{A} is Hurwitz.

Consider a Lyapunov function candidate,

$$V_o = \frac{1}{2} \bar{\sigma}^T \bar{P} \bar{\sigma} \tag{33}$$

where \bar{P} is a symmetric positive definite matrix satisfying

$$\bar{A}^T \bar{P} + \bar{P} \bar{A} = -\bar{Q} \tag{34}$$

where \bar{Q} is a symmetric positive definite matrix.

Differentiating (33) gives

$$\dot{V}_o = \frac{1}{2} \bar{\sigma}^T \bar{P} \dot{\bar{\sigma}} + \frac{1}{2} \dot{\bar{\sigma}}^T \bar{P} \bar{\sigma} \tag{35}$$

Substituting (32) and (34) in (35) gives

$$\dot{V}_o = -\frac{1}{2}\bar{\sigma}^T \bar{Q} \bar{\sigma} + \frac{1}{2}(\bar{\sigma}^T \bar{P} \bar{\delta} + \bar{\delta}^T \bar{P} \bar{\sigma}) \quad (36)$$

Assume that $\bar{\delta} \leq \gamma \|\bar{\sigma}\|_2$, where γ is a positive constant gain. Thus, the above equation becomes

$$\dot{V}_o \leq -\frac{1}{2}\|\bar{\sigma}\|^2 \|\bar{Q}\| + \gamma \|\bar{\sigma}\|^2 \|\bar{P}\| \quad (37)$$

$$\dot{V}_o \leq -\|\bar{\sigma}\|^2 \left(\frac{1}{2} \lambda_{\min} \bar{Q} - \gamma \lambda_{\max} \bar{P} \right) \quad (38)$$

where λ_{\min} represents the minimum Eigen-values of \bar{Q} and λ_{\max} illustrates the maximum Eigen-values of \bar{P} . If $\lambda_{\min} \bar{Q} > 2\gamma \lambda_{\max} \bar{P}$, then $\dot{V}_o \leq -\bar{\gamma} V_o$. Thus, the exponential convergence of sliding surface $\bar{\sigma}$ to zero has been guaranteed. Finally, V_o in (38) is negative as long as

$$\dot{V}_o \leq -\bar{\gamma} \|\bar{\sigma}\|^2 \quad (39)$$

where $\bar{\gamma} = \frac{1}{2} \lambda_{\min} \bar{Q} - \gamma \lambda_{\max} \bar{P}$.

Thus, the SMO is designed for the highly precise state estimations in the presence of nonlinearity, frictions, and external disturbances. These nonlinear frictions and external disturbances are approximated using NFDO in the next section.

NONLINEAR FRICTION AND DISTURBANCE OBSERVER (NFDO) DESIGN

The effects of frictions and disturbances have been considered in the plant model to increase the accuracy in mechanical modelling of VSWT. The exact measurement process of nonlinear friction and external disturbances present in the VSWT model is a very difficult task. To estimate these uncertainties, an NFDO is designed in this section, which deals with the frictional effect existing across the rotor and generator shaft including the presence of external disturbances occurred in the VSWT.

The nonlinear model of VSWT (22) is depicted in a generalized form and is given as

$$\begin{aligned} \dot{x} &= f(x, v_w^r) + gu + T_{Fd}(x) \\ y &= h(x) \end{aligned} \quad (40)$$

where $T_{Fd}(x, t)$ is considered to be unknown. For the estimation of $T_{Fd}(x)$, the nonlinear friction and disturbance observer (Zhou *et al.*, 2015) are designed as

$$\hat{T}_{Fd}(x, t) = X + \Gamma(x) \quad (41)$$

$$\dot{X} = -D_f \left[X + \Gamma(x) + f(x, v_w^r) + gu \right] \quad (42)$$

where $X \in \mathfrak{R}^8$ = internal state of NFDO, $\Gamma(x) \in \mathfrak{R}^8$ = designed function vector which force the NFDO gain $D_f \in \mathfrak{R}^{8 \times 8} = \frac{\partial \Gamma(x)}{\partial x}$ to satisfy $2\lambda_{\min}(D_f) - 1 > 0$.

The estimation error of the NFDO is given as

$$\tilde{T}_{Fd} = T_{Fd} - \hat{T}_{Fd} \quad (43)$$

Differentiating (43) gives

$$\dot{\tilde{T}}_{Fd} = \dot{T}_{Fd} - \dot{\hat{T}}_{Fd} = \dot{T}_{Fd} - \dot{X} - \frac{\partial \Gamma(x)}{\partial x} \dot{x} \quad (44)$$

Using (40) and (42), (44) becomes

$$\dot{\tilde{T}}_{Fd} = \dot{T}_{Fd} + D_f (X + \Gamma - T_{Fd}) \quad (45)$$

Again, using (41) and (43) gives

$$\dot{\tilde{T}}_{Fd} = \dot{T}_{Fd} - D_f \tilde{T}_{Fd} \quad (46)$$

Theorem 1: Consider the VSWT uncertain model (22) satisfying the assumption $\|\dot{T}_{Fd}(x, t)\| \leq \beta_{Fd}$; therefore the NFDO is designed as (41) and (42), then \tilde{T}_{Fd} is bounded.

Proof: Consider a Lyapunov function candidate,

$$V_{T_{Fd}} = \frac{1}{2} \tilde{T}_{Fd}^T \tilde{T}_{Fd} \quad (47)$$

Differentiating (47),

$$\dot{V}_{T_{Fd}} = -\tilde{T}_{Fd}^T D_f \tilde{T}_{Fd} + \tilde{T}_{Fd}^T \dot{\tilde{T}}_{Fd} \quad (48)$$

Assume that $\|\dot{\tilde{T}}_{Fd}(x, t)\| \leq \beta_{Fd}$; therefore (Zhou *et al.*, 2015)

$$\dot{V}_{T_{Fd}} \leq -\tilde{T}_{Fd}^T D_f \tilde{T}_{Fd} + \frac{1}{2} \tilde{T}_{Fd}^T \tilde{T}_{Fd} + \frac{1}{2} \beta_{Fd}^2 \quad (49)$$

$$\dot{V}_{T_{Fd}} \leq -\underbrace{\left\{2\lambda_{\min}(D_f) - 1\right\}}_K V_{T_{Fd}} + \frac{1}{2} \beta_{Fd}^2 \quad (50)$$

Integrating (50) gives

$$0 \leq V_{T_{Fd}} \leq \frac{M}{K} + \left(V_{T_{Fd}}(0) - \frac{M}{K} \right) e^{-Kt} \quad (51)$$

$$\|\tilde{T}_{Fd}\| \leq \sqrt{2V_{T_{Fd}}} \leq \sqrt{2 \left(\frac{M}{K} + \left| V_{T_{Fd}}(0) - \frac{M}{K} \right| \right)} \quad (52)$$

It assists the estimation of $T_{Fd}(x)$ which results in the reduction of stress on VSWT due to the random behavior of wind speed. In order to achieve the control objectives, an adaptive quasi-sliding mode control has been designed with the consideration of the effect of friction and external disturbances in the next section.

SMO and NFDO BASED ADAPTIVE CONTROLLER DESIGN

In order to carry out the observer based adaptive controller design for VSWT, the nonlinear plant model (22) and SMO (25) have been transformed into the approximate normal form (Slotine *et al.* 1991). The normal form modeling of VSWT is considered to ensure the notions of internal dynamics as well as zero-dynamics of the plant (Byrnes *et al.* 1984).

Normal form modeling of VSWT:

The relative degree of VSWT system (22) for torque control (Region 2) and pitch control (Region 3) is obtained as $\{3, 3\}$. Now, considering $Z = [h(x) \quad L_f h(x) \quad L_f^2 h(x)]^T \equiv [Z_1 \quad Z_2 \quad Z_3]^T$, where,

$$h(x) = x_1, \quad L_f h(x) = \bar{f}_1 + A_{11}x_1 + A_{12}x_2 + A_{13}x_3 \quad \text{and} \quad L_f^2 h(x) = \left[\left\{ A_{11} + \frac{\partial \bar{f}_1}{\partial x_1} \right\} A_{11} + A_{12}A_{21} + A_{13} \right] x_1 \\ + \left[\left\{ A_{11} + \frac{\partial \bar{f}_1}{\partial x_1} \right\} A_{12} + A_{12}A_{22} + A_{13}A_{32} \right] x_2 + \left[\left\{ A_{11} + \frac{\partial \bar{f}_1}{\partial x_1} \right\} A_{13} + A_{12}A_{23} \right] x_3 + A_{12}A_{28}x_8 + \frac{\partial \bar{f}_1}{\partial x_6} x_7 + \left\{ A_{11} + \frac{\partial \bar{f}_1}{\partial x_1} \right\} \bar{f}_1$$

and $L_g L_f h(x) = 0$.

The VSWT system (22) can be rewritten in the approximate normal form as

$$\dot{Z} = \begin{bmatrix} L_f h(x) \\ L_f^2 h(x) + L_g L_f h(x) \\ L_f^3 h(x) + L_g L_f^2 h(x) u_c \end{bmatrix} \equiv \begin{bmatrix} Z_2 + T_{Fd_1}(Z, t) \\ Z_3 + \bar{T}_{Fd_2}(Z, t) \\ \bar{b}(Z) + \bar{a}(Z) u_c + \bar{T}_{Fd_3}(Z, t) \end{bmatrix} \quad (53)$$

$$y = h(x) \equiv Z_1$$

where $\bar{T}_{Fd}(Z, t)$ represents the transformed form of uncertainty term $T_{Fd}(x, t)$,

$$\bar{a}(Z) = A_{12}A_{28}g_8, \quad u_c = u_2 = T_{g.ref} \quad (\text{for TCR in Region II}),$$

$$\bar{a}(Z) = \frac{\partial \bar{f}_1}{\partial x_6} g_7, \quad u_c = u_1 = \theta_{ref} \quad (\text{for PCR in Region III}),$$

$$\bar{b}(Z) = \left\{ A_{11} \frac{\partial \bar{f}_1}{\partial x_1} + \left(\frac{\partial \bar{f}_1}{\partial x_1} \right)^2 + \frac{\partial^2 \bar{f}_1}{\partial x_1^2} \bar{f}_1 + A_{11}^2 + \frac{\partial^2 \bar{f}_1}{\partial x_1^2} A_{11}x_1 + \frac{\partial \bar{f}_1}{\partial x_1} A_{11} + A_{12}A_{21} + A_{13} \right\} (\bar{f}_1 + A_{11}x_1 + A_{12}x_2 + A_{13}x_3) \\ + \left\{ A_{11}A_{12} + \frac{\partial \bar{f}_1}{\partial x_1} A_{12} + A_{12}A_{22} + A_{13}A_{32} \right\} (A_{21}x_1 + A_{22}x_2 + A_{23}x_3 + A_{28}x_8) + \left\{ A_{11}A_{13} + \frac{\partial \bar{f}_1}{\partial x_1} A_{13} + A_{12}A_{23} \right\} \times \\ (x_1 + A_{32}x_2) + \frac{\partial^2 \bar{f}_1}{\partial x_6^2} x_7^2 + \frac{\partial \bar{f}_1}{\partial x_6} (A_{76}x_6 + A_{77}x_7) + A_{12}A_{28}A_{88}x_8.$$

The nonlinear terms that appeared in $\bar{b}(Z)$ are given as follows:

$$\frac{\partial \bar{f}_1}{\partial x_1} = \frac{0.5\rho\pi R^2 v_w^3}{J_r} \left\{ \frac{1}{x_1} \frac{\partial C_p(\lambda, x_6)}{\partial x_1} - \frac{C_p(\lambda, x_6)}{x_1^2} \right\} \quad (54)$$

$$\text{where} \quad \frac{\partial C_p}{\partial x_1} = \frac{\pi R / v_w}{18 - 0.3(x_6 - 2)} \{0.5 - 0.0167(x_6 - 2)\} \cos \left\{ \frac{\pi(x_1 R / v_w + 0.1)}{18 - 0.3(x_6 - 2)} \right\} - 0.00184(R / v_w)(x_6 - 2).$$

$$\frac{\partial^2 \bar{f}_1}{\partial x_1^2} = \frac{0.5\rho\pi R^2 v_w^3}{J_r} \left\{ \frac{C_p(\lambda, x_6)}{x_1^3} + \frac{1}{x_1} \frac{\partial^2 C_p(\lambda, x_6)}{\partial x_1^2} \right\} \quad (55)$$

$$\text{where } \frac{\partial^2 C_p}{\partial x_1^2} = - \left\{ \frac{\pi R / v_w}{18 - 0.3(x_6 - 2)} \right\}^2 \{0.5 - 0.0167(x_6 - 2)\} \sin \left\{ \frac{\pi(x_1 R / v_w + 0.1)}{18 - 0.3(x_6 - 2)} \right\}.$$

$$\frac{\partial \bar{f}_1}{\partial x_6} = \frac{0.5 \rho \pi R^2 v_w^3}{J_r} \frac{1}{x_1} \frac{\partial C_p(\lambda, x_6)}{\partial x_6} \quad (56)$$

$$\text{where } \frac{\partial C_p}{\partial x_6} = \frac{0.3 \pi (x_1 R / v_w + 0.1)}{(18 - 0.3(x_6 - 2))^2} \{0.5 - 0.0167(x_6 - 2)\} \cos \left\{ \frac{\pi(x_1 R / v_w + 0.1)}{18 - 0.3(x_6 - 2)} \right\} - 0.00184(x_1 R / v_w - 3).$$

$$- 0.0167 \sin \left\{ \frac{\pi(x_1 R / v_w + 0.1)}{18 - 0.3(x_6 - 2)} \right\}.$$

$$\frac{\partial^2 \bar{f}_1}{\partial x_6^2} = \frac{0.5 \rho \pi R^2 v_w^3}{J_r} \frac{1}{x_1} \frac{\partial^2 C_p(\lambda, x_6)}{\partial x_6^2} \quad (57)$$

$$\text{where } \frac{\partial^2 C_p}{\partial x_6^2} = \frac{0.09 \pi (x_1 R / v_w + 0.1)}{(18 - 0.3(x_6 - 2))^3} \{0.5 - 0.0167(x_6 - 2)\} \cos \left\{ \frac{\pi(x_1 R / v_w + 0.1)}{18 - 0.3(x_6 - 2)} \right\} - \{0.5 - 0.0167(x_6 - 2)\}$$

$$\times \left\{ \frac{0.3 \pi (x_1 R / v_w + 0.1)}{(18 - 0.3(x_6 - 2))^2} \right\}^2 \sin \left\{ \frac{\pi(x_1 R / v_w + 0.1)}{18 - 0.3(x_6 - 2)} \right\} - 0.0167 \cos \left\{ \frac{\pi(x_1 R / v_w + 0.1)}{(18 - 0.3(x_6 - 2))^2} \right\}$$

$$\times \left\{ \frac{0.3 \pi (x_1 R / v_w + 0.1)}{(18 - 0.3(x_6 - 2))^2} \right\} + 0.0167 \cos \left\{ \frac{\pi(x_1 R / v_w + 0.1)}{18 - 0.3(x_6 - 2)} \right\} \left\{ \frac{\pi(x_1 R / v_w + 0.1)}{(18 - 0.3(x_6 - 2))^2} \right\}.$$

Similarly, the SMO (25) for VSWT system (53) can be transformed into approximate normal form as

$$\dot{\hat{Z}} = \begin{bmatrix} L_f h(\hat{x}) \\ L_f^2 h(\hat{x}) + L_g L_f h(\hat{x}) \\ L_f^3 h(\hat{x}) + L_g L_f^2 h(\hat{x}) u_c \end{bmatrix} \equiv \begin{bmatrix} \hat{Z}_2 \\ \hat{Z}_3 \\ \bar{b}(\hat{Z}) + \bar{a}(\hat{Z}) u_c \end{bmatrix} \quad (58)$$

$$\hat{y} = h(\hat{x}) \equiv \hat{Z}_1$$

where \hat{Z} is the estimate of Z and the state estimation error terms $\tilde{Z} = Z - \hat{Z}$ are negligible after a short transient.

Adaptive sliding mode controller (SMC) design:

The adaptive sliding mode controller based on NFDO (42) and SMO (58) for the VSWT is designed in this subsection. Considering the sliding surface,

$$S = \ddot{e} + 2\lambda \dot{e} + \lambda^2 e, \quad (59)$$

where $e = Z_1 - Z_{1d}$ is the reference tracking error, λ is the positive constant, and Z_{1d} is the desired rotor speed as reference trajectory. The reference tracking error can be rewritten as $e = \tilde{Z}_1 + \hat{Z}_1 - Z_{1d}$. Differentiating (59) gives

$$\dot{S} = \ddot{e} + 2\lambda \dot{e} + \lambda^2 \dot{e}, \quad (60)$$

where, $\dot{e} = \dot{\hat{Z}}_1 + \dot{\hat{Z}}_2 - \dot{Z}_{1d}$, $\ddot{e} = \ddot{\hat{Z}}_1 + \ddot{\hat{Z}}_3 - \ddot{Z}_{1d}$, $\ddot{e} = \ddot{\hat{Z}}_1 + \bar{b}(\hat{Z}) + \bar{a}(\hat{Z})u_c - \ddot{Z}_{1d}$. The error function dynamics of the sliding surface (59) are given by.

$$\dot{S} = \left\{ \ddot{\hat{Z}}_1 + 2\lambda\ddot{\hat{Z}}_1 + \lambda^2\dot{\hat{Z}}_1 \right\} + \bar{b}(\hat{Z}) + \bar{a}(\hat{Z})u_c - \ddot{Z}_{1d} + 2\lambda(\dot{\hat{Z}}_3 - \dot{Z}_{1d}) + \lambda^2(\dot{\hat{Z}}_2 - \dot{Z}_{1d}) \quad (61)$$

$$\dot{S} = \Upsilon_b + \Upsilon_a u_c - \ddot{Z}_{1d} + 2\lambda(\dot{\hat{Z}}_3 - \dot{Z}_{1d}) + \lambda^2(\dot{\hat{Z}}_2 - \dot{Z}_{1d}) \quad (62)$$

where $\Upsilon_a = \bar{a}(\hat{Z})$, $\Upsilon_b = \left\{ \ddot{\hat{Z}}_1 + 2\lambda\ddot{\hat{Z}}_1 + \lambda^2\dot{\hat{Z}}_1 \right\} + \bar{b}(\hat{Z})$.

The sliding mode control law can be chosen as

$$u_c = \left[\hat{\Upsilon}_a \right]^{-1} \left[-\hat{\Upsilon}_b + \ddot{Z}_{1d} - 2\lambda(\dot{\hat{Z}}_3 - \dot{Z}_{1d}) - \lambda^2(\dot{\hat{Z}}_2 - \dot{Z}_{1d}) + u_r \right] \quad (63)$$

where $\hat{\Upsilon}_a$ and $\hat{\Upsilon}_b$ are the estimates of Υ_a and Υ_b respectively, $u_r = -K_r \text{sgn}(S)$ with $K_r > 0$. The sliding mode control efforts are $\theta_{ref} = u_1 = 0$ and $T_{g,ref} = u_2 = u_c$ for torque control and $\theta_{ref} = u_1 = u_c$ and $T_{g,ref} = u_2 = 40680.17\text{N-m}$ for pitch control.

Substituting (63) in (62)

$$\dot{S} = \tilde{\Upsilon}_b + \tilde{\Upsilon}_a u_c + u_r \quad (64)$$

where $\tilde{\Upsilon}_b = \Upsilon_b - \hat{\Upsilon}_b$, $\tilde{\Upsilon}_a = \Upsilon_a - \hat{\Upsilon}_a$.

In the VSWT control system, it is essential to avoid the chattering effect of controller by providing a smooth/continuous control signal. The VSWT cannot perform well with high frequency chattering, but it is desirable to retain the robustness/insensitivity of the control system in the presence of system uncertainties. One of the solutions to make the control signal (63) smooth/continuous is to approximate the discontinuous function u_r by some smooth/continuous function (e.g., sigmoid function). However, this smooth control function cannot provide finite time convergence of the switching surface and state variables to zero in the presence of system uncertainty and external disturbances (Shtessel *et al.*, 2014). Also, this smooth control function provides loss of robustness and accuracy. Thus, the performance of VSWT using smooth control law (with sigmoid function) is close to the discontinuous control law (63). In the quasi-sliding mode control, the idea is to design the control law in terms of derivative of the control function where the sliding surface converges to the vicinity of origin. In the QSMC, the actual control law, which is the integral of a high frequency switching function that is continuous. Thus, this approach is called chattering attenuation method.

Adaptive quasi-sliding mode controller (QSMC) design:

To attenuate the chattering, an auxiliary sliding variable is defined as

$$\bar{S} = \dot{S} + \bar{\lambda}S \quad (65)$$

By differentiating (65), we obtained this

$$\dot{\bar{S}} = \ddot{S} + \bar{\lambda}\dot{S} \quad (66)$$

where $\dot{S} = (\Upsilon_b + \Upsilon_a u_c - \ddot{Z}_{1d}) + 2\lambda(\dot{\hat{Z}}_3 - \dot{Z}_{1d}) + \lambda^2(\dot{\hat{Z}}_2 - \dot{Z}_{1d})$ and $\ddot{S} = (\dot{\Upsilon}_b + \Upsilon_a \dot{u}_c + \dot{\Upsilon}_a u_c - \ddot{\Upsilon}_b) + 2\lambda(\dot{\hat{Z}}_3 - \dot{Z}_{1d}) + \lambda^2(\dot{\hat{Z}}_2 - \dot{Z}_{1d})$.

Let $\dot{u}_c = \bar{u}_c$ be the quasi-sliding mode control input, then (66) becomes

$$\ddot{\bar{S}} = \{\Upsilon_c - \ddot{Z}_{1d}\} + \Upsilon_a \bar{u}_c + (2\lambda + \bar{\lambda})\{\Upsilon_b + \Upsilon_a u_c - \ddot{Z}_{1d}\} + (\lambda^2 + 2\bar{\lambda}\lambda)(\hat{Z}_3 - \ddot{Z}_{1d}) + \bar{\lambda}\lambda^2(\hat{Z}_2 - \dot{Z}_{1d}) \quad (67)$$

where $\Upsilon_c = \dot{\Upsilon}_b + \dot{\Upsilon}_a u_c$.

The quasi-sliding mode control law can be chosen as

$$\bar{u}_c = [\hat{\Upsilon}_a]^{-1} \left[-\hat{\Upsilon}_c + \ddot{Z}_{1d} - (2\lambda + \bar{\lambda})\{\hat{\Upsilon}_b + \hat{\Upsilon}_a u_c - \ddot{Z}_{1d}\} - (\lambda^2 + 2\bar{\lambda}\lambda)(\hat{Z}_3 - \ddot{Z}_{1d}) - \bar{\lambda}\lambda^2(\hat{Z}_2 - \dot{Z}_{1d}) + \bar{u}_r \right] \quad (68)$$

where $\bar{u}_r = -\bar{K}_r \operatorname{sgn}(\bar{S})$ with $\bar{K}_r > 0$. The quasi-sliding mode control efforts are $\theta_{ref} = u_1 = 0$ and $T_{g,ref} = u_2 = \int_0^t \bar{u}_c dt$ for torque control in Region II and $\theta_{ref} = u_1 = \int_0^t \bar{u}_c dt$ and $T_{g,ref} = u_2 = 40680.17 \text{N-m}$ for pitch control in Region III.

Substituting (68) in (67)

$$\ddot{\bar{S}} = \tilde{\Upsilon}_c + (2\lambda + \bar{\lambda})\{\tilde{\Upsilon}_b + \tilde{\Upsilon}_a u_c\} + \bar{u}_r \quad (69)$$

where $\tilde{\Upsilon}_c = \Upsilon_c - \hat{\Upsilon}_c$.

The unknown nonlinear functions Υ_a , Υ_b , and Υ_c can be approximated as $\hat{\Upsilon}_a$, $\hat{\Upsilon}_b$, and $\hat{\Upsilon}_c$ using RBFNN and are given as

$$\Upsilon_a = W_a^T \phi_a(Z, \hat{Z}, V_w) + \varepsilon_a, \quad \Upsilon_b = W_b^T \phi_b(Z, \hat{Z}, V_w) + \varepsilon_b, \quad \Upsilon_c = W_c^T \phi_c(Z, \hat{Z}, V_w, u_c) + \varepsilon_c \quad (70)$$

$$\text{and} \quad \hat{\Upsilon}_a = \hat{W}_a^T \phi_a(Z, \hat{Z}, V_w), \quad \hat{\Upsilon}_b = \hat{W}_b^T \phi_b(Z, \hat{Z}, V_w), \quad \hat{\Upsilon}_c = \hat{W}_c^T \phi_c(Z, \hat{Z}, V_w, u_c), \quad (71)$$

where ε_a , ε_b , ε_c , are the approximation errors of RBFNN which are bounded, \hat{W}_a , \hat{W}_b , \hat{W}_c are the estimate of the optimal weights W_a , W_b , W_c of RBFNN, and ϕ_a , ϕ_b , ϕ_c are the basis function. These optimal weights are bounded as $\|W_a\|_F \leq W_A$, $\|W_b\|_F \leq W_B$, $\|W_c\|_F \leq W_C$, where $W_A > 0$, $W_B > 0$, $W_C > 0$, and $\|\cdot\|_F$ is the Frobenius norm (Lewis *et al.*, 1998).

Theorem 2: If the desired rotor speed output Z_{1d} is bound up to its fourth order derivatives, and the weights of RBFNN used in the observer based controller (68) for the VSWT plant (53) are updated according to the adaptation laws,

$$\dot{\hat{W}}_a = \eta_1 \phi_a \bar{S} - \rho \eta_1 \|\bar{S}\| \hat{W}_a, \quad \dot{\hat{W}}_b = \eta_2 \phi_b \bar{S} - \rho \eta_2 \|\bar{S}\| \hat{W}_b, \quad \dot{\hat{W}}_c = \eta_3 \phi_c \bar{S} - \rho \eta_3 \|\bar{S}\| \hat{W}_c \quad (72)$$

where ρ is the damping coefficient, η_1 , η_2 , η_3 are the learning rates of RBFNN-1 ($\hat{\Upsilon}_a$), RBFNN-2 ($\hat{\Upsilon}_b$), RBFNN-3 ($\hat{\Upsilon}_c$) respectively, then the sliding surface \bar{S} and RBFNN weight estimation errors are uniformly ultimately bounded.

$$\dot{\bar{S}} = \tilde{W}_c^T \phi_c(Z, \hat{Z}, V_w) + \varepsilon_c + \mu \{\tilde{W}_b^T \phi_b(Z, \hat{Z}, V_w) + \varepsilon_b\} + \mu \{\tilde{W}_a^T \phi_a(Z, \hat{Z}, V_w) u_c + \varepsilon_a u_c\} + \bar{u}_r \quad (73)$$

where, $\tilde{W}_a = W_a - \hat{W}_a$, $\tilde{W}_b = W_b - \hat{W}_b$, $\tilde{W}_c = W_c - \hat{W}_c$ and $\mu = (2\lambda + \bar{\lambda})$.

Proof: The detailed stability analysis of observer based controller has been done and the expression of (81) is obtained, which assures that the Lyapunov function $V(t)$ is bounded (refer Appendix). The proposed robust observer based adaptive control scheme has been validated using simulation studies. The simulation results showing tracking performance with lesser tracking errors for both regions (TCR and PCR) that are demonstrated in the next section.

SIMULATION RESULTS

In this section, the proposed nonlinear robust observer based adaptive controller for VSWT is validated through detailed simulation studies with the system parameters being referred to in Table A1 given in Appendix. The block diagram of overall closed-loop robust observer based controller is depicted in Fig. 6.

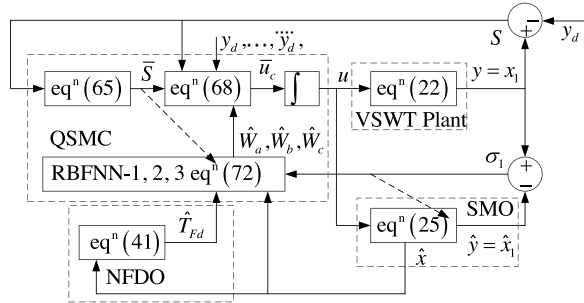


Fig. 6. Block diagram of proposed robust observer based control scheme.

Sliding mode observer:

The VSWT is operated in the open-loop with the control inputs given as $u_1 = u_2 = 0.5 \sin(0.5t)$. The initial conditions for plant and observer are taken as $[0.05 \ 0 \ 0 \ 0 \ 0 \ 0 \ 0 \ 0]$ and $[0.06 \ 0.01 \ 0 \ 0 \ 0 \ 0 \ 0 \ 0]$ respectively. The values of the sliding mode observer gains $K = [0.1 \ 0.1 \ 0.1 \ 0.1 \ 0.1 \ 0.1 \ 0.1 \ 0.1]^T$ and $\alpha = [0.1 \ 0.1 \ 0.1 \ 0.1 \ 0.1 \ 0.1 \ 0.1 \ 0.1]^T$ are chosen such that matrix \bar{A} is Hurwitz.

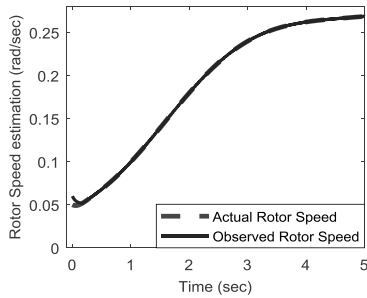


Fig. 7. Rotor Speed estimation ($\omega_r, \hat{\omega}_r$).

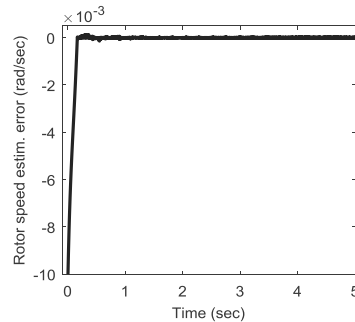


Fig. 8. Rotor Speed estimation error ($\omega_r - \hat{\omega}_r$).

The convergence of observed rotor speed with actual rotor speed is plotted in Fig. 7. The observation error between actual and observed rotor speed is shown in Fig. 8. Also, to show the superiority of SMO, the estimate of one of the unmeasurable states (generator speed) is given below.

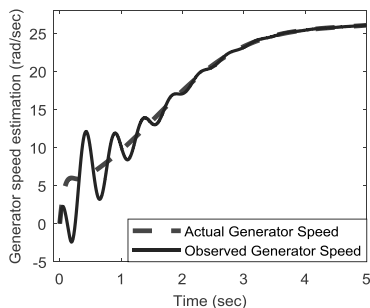


Fig. 9. Generator speed estimation ($\omega_g, \hat{\omega}_g$).

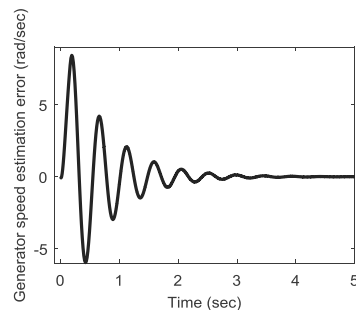


Fig. 10. Generator speed estimation error ($\omega_g - \hat{\omega}_g$).

The convergence of observed generator speed with actual generator speed is plotted in Fig. 9. The observation error between actual and observed generator speed is shown in Fig. 10. From the above plots it can be easily observed that the observer states converge to the plant states in minimum time and the error between them converges to zero very quickly. The simulation study at various initial conditions of SMO has been carried out and the error analysis based on these simulations is shown in Table 1.

Table 1. RMS value of the estimated errors with and without friction and disturbance.

Specifications	Without uncertainty	With uncertainty
Rotor speed estimation error (rad/sec)	0.00017709	0.00038772
Generator speed estimation error (rad/sec)	1.3094	3.3263

From Table 1, it is clear that the proposed SMO remains stable even in the presence of uncertainty (disturbance and frictional effect) with slight change in the estimation errors. The performance of NFDO for the approximation of external disturbances and frictions is given in the next subsection.

Nonlinear friction and disturbance observer:

The design parameters for NFDO are chosen as $F_c = 0.001$, $F_s = 0.001$, $F_v = 0.001$, $v_s = 0.001$, and $\Gamma(\hat{x}) = [(2\hat{x}_1 + 0.5) \quad (2\hat{x}_2 + 0.5) \quad \dots \quad (2\hat{x}_7 + 0.5) \quad (2\hat{x}_8 + 0.5)]^T$. The unknown and bounded time varying disturbance term for the VSWT has been taken as $d(t) = 0.1 \sin(0.5t)$. The approximation of external disturbances with friction and the error between actual and estimated terms ($\|T_{Fd}\|$ and $\|\hat{T}_{Fd}\|$) are depicted in Fig. 11 and Fig. 12.

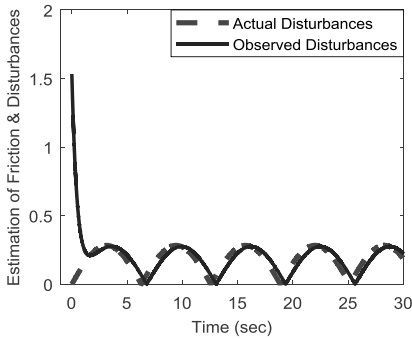


Fig. 11. Dist. and friction estimation ($\|T_{Fd}\|, \|\hat{T}_{Fd}\|$).

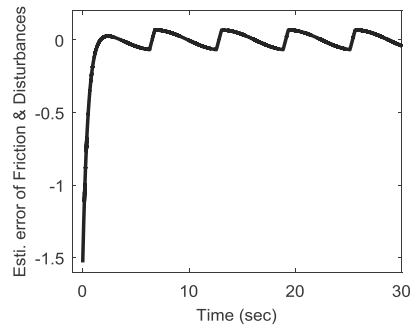


Fig. 12. Dist. and friction estimation error ($\|T_{Fd}\| - \|\hat{T}_{Fd}\|$).

From Fig. 11 and Fig. 12, it can be seen that the designed NFDO closely approximates the friction and external disturbances and approximation error finally tends to zero quickly. Based on the above simulation results, it can be said that both observers (SMO and NFDO) can realize good estimation of states as well as friction and disturbances with lesser errors.

Zero dynamics Response:

The zero dynamics response of VSWT is obtained considering the initial conditions of the plant and observer as $[0.05 \ 0 \ 0 \ 0 \ 0 \ 0 \ 0 \ 0]$ and $[0.06 \ 0.01 \ 0.1 \ 0.1 \ 0.1 \ 0.1 \ 0.1 \ 0.1]$. These responses are plotted below in Fig. 13 and Fig. 14.

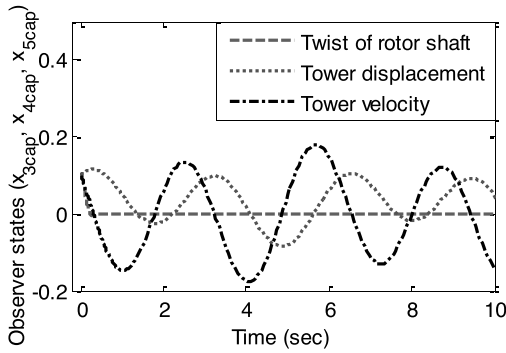


Fig. 13. Zero dynamics of states $(\hat{x}_3, \hat{x}_4, \hat{x}_5)$.

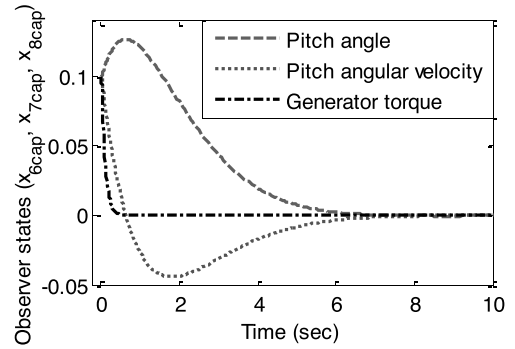


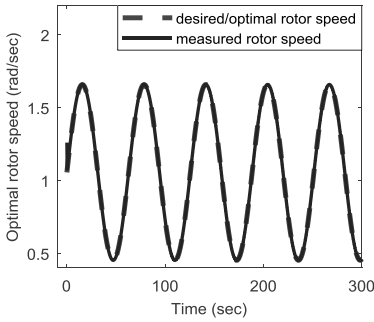
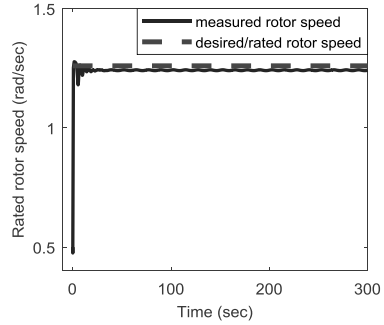
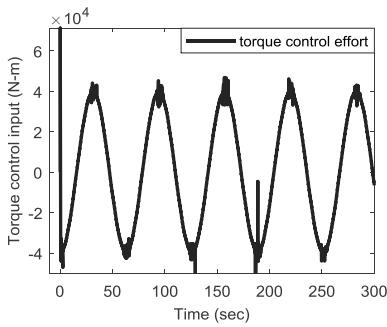
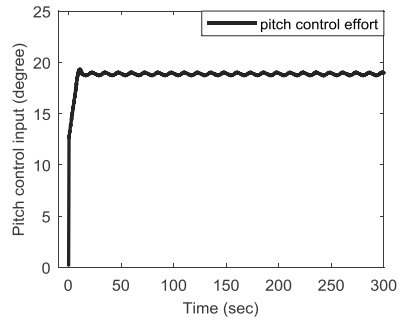
Fig. 14. Zero dynamics of states $(\hat{x}_6, \hat{x}_7, \hat{x}_8)$.

These plots are showing the stability of zero dynamics of the VSWT and SMO whose states \hat{x} converge to their equilibrium points x_e i.e. $\lim_{t \rightarrow \infty} \|\hat{x}\| \rightarrow x_e$ (Slotine *et al.* 1991). The performance of proposed observer based controller is given in the next subsection.

Robust observer based adaptive controller:

The detailed simulation studies of proposed observer based controller are done by appropriate selection of design parameters. The initial conditions of VSWT nonlinear plant and observer are selected as $[1.26 \ 0 \ 0 \ 0 \ 0 \ 0 \ 0 \ 0 \ 0]$ and $[0.5 \ 0 \ 0 \ 0 \ 0 \ 0 \ 0 \ 0 \ 0]$ respectively. The wind speeds are considered as $4\sin(0.1t) + 7$ (varying from cut-in wind speed 3 m/sec to rated wind speed 11 m/sec) for TCR and $7\sin(0.1t) + 18$ (varying from rated wind speed 11 m/sec to cut-out wind speed 25 m/sec) for PCR, respectively. The reference trajectories are selected as the optimal rotor speed $\omega_{r_{opt}} = (9.5/63)\{4\sin(0.1t) + 7\}$ for torque control (TCR) of region II and the rated rotor speed $\omega_{r_{rated}} = 1.26$ for pitch control (PCR) of region III.

The controller design parameters are chosen as $\lambda = 50$, $\bar{\lambda} = 50$ and $\bar{K}_r = 15$ for TCR and $\lambda = 80$, $\bar{\lambda} = 75$ and $\bar{K}_r = 81$ for PCR, respectively. The RBFNN weights are initially selected randomly 0.1 or 0.2. The neural networks tuning parameters are chosen as $\eta_1 = 0.001$, $\eta_2 = 0.001$, $\eta_3 = 0.001$, $\rho = 0.1$. The inputs to the RBFNN-1 (\hat{Y}_a) are x_1 , \hat{x}_1 , \hat{x}_5 , \hat{x}_6 , and v_w . The basis function $\phi_a(Z, \hat{Z}, V_w, u_c)$ and the weight of RBFNN-1 (\hat{W}_a) have the dimensions of (5×1) and (5×1) , respectively. Thus, the total no. of weights required to be updated for the estimation of nonlinear function \hat{Y}_a is 5. Similarly, the inputs to the RBFNN-2 (\hat{Y}_b) are x_1 , \hat{x}_1 , \hat{x}_2 , \hat{x}_3 , \hat{x}_4 , \hat{x}_5 , \hat{x}_6 , \hat{x}_7 , \hat{x}_8 , and v_w . The basis function $\phi_b(Z, \hat{Z}, V_w, u_c)$ and the weight of RBFNN-2 (\hat{W}_b) have the dimensions of (10×1) and (10×1) , respectively. Thus, the total no. of weights required to be updated for the estimation of nonlinear function \hat{Y}_b is 10. Correspondingly, the inputs to the RBFNN-3 (\hat{Y}_c) are x_1 , \hat{x}_1 , \hat{x}_2 , \hat{x}_3 , \hat{x}_4 , \hat{x}_5 , \hat{x}_6 , \hat{x}_7 , \hat{x}_8 , v_w , and u_c . The basis function $\phi_c(Z, \hat{Z}, V_w, u_c)$ and the weight of RBFNN-3 (\hat{W}_c) have the dimensions of (11×1) and (11×1) , respectively. Thus, the total no. of weights required to be updated for the estimation of nonlinear function \hat{Y}_c is 11. The tracking performance of the proposed QSMC based controller for the nonlinear model of the VSWT has been demonstrated below.


Fig. 15. Rotor speed tracking for TCR (ω_{opt} , ω_r).

Fig. 16. Rotor speed tracking for PCR (ω_{rated} , ω_r).

Fig. 17. Torque control effort ($u_2 = T_{g,ref}$).

Fig. 18. Pitch control effort ($u_1 = \theta_{ref}$).

The above simulation results demonstrate that the system output follows the desired response in a satisfactory way, even in the presence of disturbance and friction. The tracking performances of the actual rotor speed with the desired trajectories (optimal/rated speed) are shown in Fig. 15 and Fig. 16. The torque and pitch control efforts are bounded within the actuator limits ($|T_{g,ref}| \leq 7.12656 \times 10^4$ N-m and $0 < \theta_{ref} \leq 25$ deg) plotted in Fig. 17 and Fig. 18, respectively.

Comparison of adaptive QSMC with other controllers:

The comparison has been made on the basis of error analysis with/without uncertainties and obtained output power from the wind. The comparative analysis for the maximum power production of the VSWT nonlinear model has been done with an existing standard wind turbine controller (SWTC). To extract the VSWT operating at peak of the $C_{p_{max}}$ curve, the SWTC law is given by Merida *et al.*, 2012; Merida *et al.*, 2014,

$$u_2 = T_{g,ref} = (K_{opt} \omega_r^2 - D_t \omega_r) / \eta_g \quad (84)$$

where $K_{opt} = 0.5\pi\rho R^5 C_{p_{max}} / \lambda_{opt}^3$. This physical law ensures the operation of VSWT close to the maximum power output in the Region II.

For the comparative evaluation in Region III, an existing proportional-integral controller (PI) based pitch control law (Singh *et al.*, 2018) is considered to hold the rotor speed constant and to achieve constant power available from wind given as

$$u_1 = \theta_{ref} = K_p e_1 + K_i \int_0^t e_1 dt \quad (85)$$

where $e_1 = \omega_r - \omega_{rated}$. The tuning parameters of PI controller (85) are selected as $K_p = -1.024$ and $K_i = -1.01$.

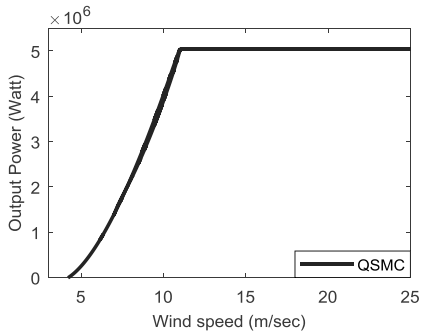


Fig. 19. Power output Vs Wind speed (QSMC).

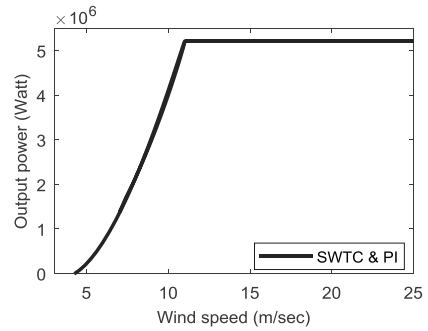


Fig. 20. Power output Vs Wind speed (SWTC & PI).

The output power with respect to wind speed has been plotted for the considered VSWT using the proposed QSMC (68) and SWTC (84) in Fig. 19 and Fig. 20. On comparing both plots it can be concluded that maximum power output has been achieved from the wind using the proposed QSMC and is almost equivalent to the SWTC. There are several simulations of the proposed control scheme that have been done for the considered VSWT. However, the results presented here are for the specific case due to the scope of the paper. For the error analysis of QSMC with SWTC and PI controller, an QFT based controller is also considered (Singh *et al.*, 2018) and is given as

$$\text{For Region II, } u_2 = \frac{-9598s^2 - 4.804 \times 10^5 s - 250.2}{s^2 + 1.468s} \tag{86a}$$

$$\text{For Region III, } u_1 = \frac{-2.497 \times 10^5 s^2 - 2.971 \times 10^6 s - 7855}{s^2 + 1.118s} \tag{86b}$$

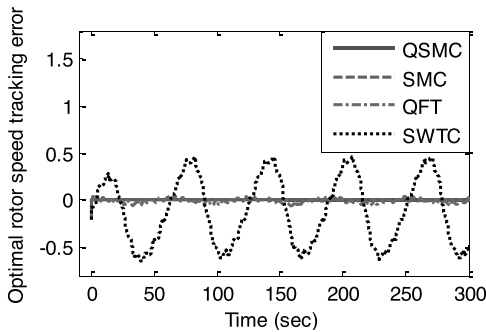


Fig. 21. Rotor speed tracking error for TCR ($\omega_r - \omega_{r_{opt}}$).

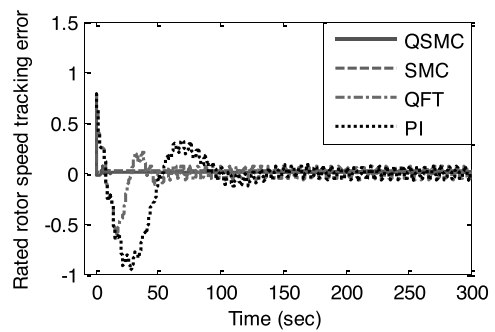


Fig. 22. Rotor speed tracking error for PCR ($\omega_r - \omega_{r_{rated}}$).

The rotor speed tracking errors with various controllers (SWTC, QFT, PI, SMC, and QSMC) are plotted in Fig. 21 and Fig. 22. Based on the above simulation studies, the reference tracking error analysis of rotor speed for both control regions is tabulated as follows.

Table 2. RMS value of the tracking errors for torque and pitch control regions for VSWT.

Rotor Speed Tracking Error	Torque Control (Region II)				Pitch Control (Region III)			
	SWTC	QFT	SMC	QSMC	PI	QFT	SMC	QSMC
With uncertainty	0.3904	0.0959	0.0120	0.0113	0.2797	0.2146	0.1470	0.0298
Without uncertainty	0.3735	0.0245	0.0115	0.0101	0.2618	0.1294	0.1427	0.0259

From Table 2, it is clearly observed that the tracking error of rotor speed in case of proposed QSMC is lowest as compared with the case of SWTC, QFT, and SMC for torque control and also for pitch control using PI, QFT, SMC in the presence of uncertainty. The proposed QSMC based controller has superior performance over SWTC, PI, QFT, and SMC based controllers. Thus, it is concluded that the closed-loop VSWT control system is showing robust performance using the proposed QSMC in terms of external disturbances, parametric uncertainty, and initial conditions.

CONCLUSION

In this paper, a robust observer based adaptive controller for three-blade horizontal axes VSWT has been developed. Due to the inaccessibility of all the plant states, a sliding mode observer is designed. The friction effect across the rotor and generator shafts of VSWT has been considered in the plant model. To reduce the effect of friction as well as external disturbances, an NFDO is intended. On the basis of SMO and NFDO, an adaptive controller is proposed using QSMC technique. The proposed observer based controller of VSWT is implemented (i) for torque control of optimal rotor speed to obtain the maximum power in region II, and (ii) for pitch control of rated rotor speed to sustain the constant rated power in region III. The unknown nonlinearities present in the VSWT plant are approximated by RBFNN through online update of the weights. The stability analysis of overall system has been done using Lyapunov theory. The simulation results clearly reflect the effectiveness of the proposed approach such as good tracking performance, fast convergence of states, better approximations, fast disturbance rejection, lesser tracking and estimation errors, and bounded control efforts. Finally, the performance of the proposed observer based controller of VSWT is compared with that of SWTC, QFT, PI, and SMC to ensure the maximum power production.

FUTURE SCOPE OF WORK

Implementation of the proposed work on the discretized model of VSWT using type-2 fuzzy logic may be attempted for future investigation.

APPENDIX

Stability analysis

Proof of Theorem 2: Consider a Lyapunov function candidate,

$$V = \frac{1}{2}\bar{S}^2 + \frac{\mu}{2}(\tilde{W}_a^T \eta_1^{-1} \tilde{W}_a) + \frac{\mu}{2}(\tilde{W}_b^T \eta_2^{-1} \tilde{W}_b) + \frac{1}{2}(\tilde{W}_c^T \eta_3^{-1} \tilde{W}_c) \quad (74)$$

Differentiating (74) gives

$$\dot{V} = \bar{S}\dot{\bar{S}} - \mu\tilde{W}_a^T \eta_1^{-1} \dot{\tilde{W}}_a - \mu\tilde{W}_b^T \eta_2^{-1} \dot{\tilde{W}}_b - \tilde{W}_c^T \eta_3^{-1} \dot{\tilde{W}}_c \quad (75)$$

Substituting (69) and (72), (75) becomes

$$\dot{V} = \mu\rho_1 \|\bar{S}\| \tilde{W}_a^T \hat{W}_a + \mu\rho_2 \|\bar{S}\| \tilde{W}_b^T \hat{W}_b + \rho_3 \|\bar{S}\| \tilde{W}_c^T \hat{W}_c + \mu\bar{S}\varepsilon_a + \mu\bar{S}\varepsilon_b + \bar{S}\varepsilon_c + \bar{S}\bar{u}_r \quad (76)$$

Apply the following inequalities (Chang *et al.*, 2014; Pratap *et al.*, 2014; Pratap *et al.*, 2018a):

$$2\tilde{W}_a^T \hat{W}_a \geq \|\tilde{W}_a\|^2 - \|W_a\|^2, \quad 2\tilde{W}_b^T \hat{W}_b \geq \|\tilde{W}_b\|^2 - \|W_b\|^2, \quad 2\tilde{W}_c^T \hat{W}_c \geq \|\tilde{W}_c\|^2 - \|W_c\|^2$$

$$\bar{S}\varepsilon_a \leq \bar{S}^2 + \varepsilon_a^2, \quad \bar{S}\varepsilon_b \leq \bar{S}^2 + \varepsilon_b^2, \quad \bar{S}\varepsilon_c \leq \bar{S}^2 + \varepsilon_c^2$$

$$\dot{V} \leq -\bar{S}\bar{K} \frac{\bar{S}}{|\bar{S}|} + \frac{1}{2}\mu\rho_1 \|\bar{S}\| (\|\tilde{W}_a\|^2 - \|W_a\|^2) + \frac{1}{2}\mu\rho_2 \|\bar{S}\| (\|\tilde{W}_b\|^2 - \|W_b\|^2) + \frac{1}{2}\rho_3 \|\bar{S}\| (\|\tilde{W}_c\|^2 - \|W_c\|^2)$$

$$+ \mu(\bar{S}^2 + \varepsilon_a^2) + \mu(\bar{S}^2 + \varepsilon_b^2) + (\bar{S}^2 + \varepsilon_c^2) \quad (77)$$

$$\begin{aligned} \dot{V} \leq & - \left\{ \frac{\bar{K}}{|\bar{S}|} - 1 - 2\mu \right\} \bar{S}^2 + \mu \left\{ \varepsilon_a^2 - \frac{1}{2} \rho_1 \|\bar{S}\| \|W_a\|^2 \right\} + \mu \left\{ \varepsilon_b^2 - \frac{1}{2} \rho_2 \|\bar{S}\| \|W_b\|^2 \right\} + \left\{ \varepsilon_c^2 - \frac{\rho_3}{2} \|\bar{S}\| \|W_c\|^2 \right\} \\ & + \frac{\mu}{2} \rho_1 \|\bar{S}\| \|\tilde{W}_a\|^2 + \frac{\mu}{2} \rho_2 \|\bar{S}\| \|\tilde{W}_b\|^2 + \frac{\rho_3}{2} \|\bar{S}\| \|\tilde{W}_c\|^2 \end{aligned} \quad (78)$$

Suppose that the above terms are bounded by (Chang *et al.*, 2014), (Patel *et al.*, 2018)

$$\varepsilon_a^2 - \frac{1}{2} \rho_1 \|\bar{S}\| \|W_a\|^2 \leq C_{1M}, \quad \varepsilon_b^2 - \frac{1}{2} \rho_2 \|\bar{S}\| \|W_b\|^2 \leq C_{2M}, \quad \varepsilon_c^2 - \frac{\rho_3}{2} \|\bar{S}\| \|W_c\|^2 \leq C_{3M}$$

$$\begin{aligned} \dot{V} \leq & - \left\{ \frac{\bar{K}}{|\bar{S}|} - 1 - 2\mu \right\} \bar{S}^2 + \frac{\mu \rho_1 \|\bar{S}\|}{2\lambda_{\max}(\eta_1^{-1})} \tilde{W}_a^T \eta_1^{-1} \tilde{W}_a + \frac{\mu \rho_2 \|\bar{S}\|}{2\lambda_{\max}(\eta_2^{-1})} \tilde{W}_b^T \eta_2^{-1} \tilde{W}_b + \frac{\rho_3 \|\bar{S}\|}{2\lambda_{\max}(\eta_3^{-1})} \tilde{W}_c^T \eta_3^{-1} \tilde{W}_c \\ & + \mu C_{1M} + \mu C_{2M} + C_{3M} \end{aligned} \quad (79)$$

Let $C_M = \mu C_{1M} + \mu C_{2M} + C_{3M}$. Now, ρ_1 , ρ_2 , ρ_3 can be obtained from the positive definiteness of η_1 , η_2 , η_3 such

that $\frac{\bar{K}}{|\bar{S}|} - 1 - 2\mu \geq \alpha_0$, $\frac{\rho_1 \|\bar{S}\|}{2\lambda_{\max}(\eta_1^{-1})} \geq \alpha_0$, $\frac{\rho_2 \|\bar{S}\|}{2\lambda_{\max}(\eta_2^{-1})} \geq \alpha_0$, and $\frac{\rho_3 \|\bar{S}\|}{2\lambda_{\max}(\eta_3^{-1})} \geq \alpha_0$. Thus

$$\dot{V} \leq -\alpha_0 \bar{S}^2 + \alpha_0 \mu \tilde{W}_a^T \eta_1^{-1} \tilde{W}_a + \alpha_0 \mu \tilde{W}_b^T \eta_2^{-1} \tilde{W}_b + \alpha_0 \tilde{W}_c^T \eta_3^{-1} \tilde{W}_c + C_M \quad (80)$$

$$\dot{V} \leq -2\alpha_0 \left[\frac{1}{2} \bar{S}^2 + \frac{\mu}{2} (\tilde{W}_a^T \eta_1^{-1} \tilde{W}_a) + \frac{\mu}{2} (\tilde{W}_b^T \eta_2^{-1} \tilde{W}_b) + \frac{1}{2} (\tilde{W}_c^T \eta_3^{-1} \tilde{W}_c) \right] + C_M$$

$$\dot{V} \leq -2\alpha_0 V + C_M \quad (81)$$

The magnitude of $\frac{C_M}{2\alpha_0}$ can be decreased by increasing the value of α_0 , corresponding to $\dot{V} \leq 0$ (Patel *et al.*, 2018).

Taking the Laplace of the above expression,

$$sV(s) - V(0) \leq -2\alpha_0 V(s) + (C_M / s)$$

$$\text{i.e., } V(s) \leq \frac{V(0)}{s + 2\alpha_0} + \frac{C_M}{2\alpha_0} \left\{ \frac{1}{s} - \frac{1}{s + 2\alpha_0} \right\} \quad (82)$$

Taking the inverse Laplace of the above expression,

$$V(t) \leq V(0) e^{-2\alpha_0 t} + \frac{C_M}{2\alpha_0} \{1 - e^{-2\alpha_0 t}\}$$

$$\text{i.e., } V(t) \leq \frac{C_M}{2\alpha_0} + \left\{ V(0) - \frac{C_M}{2\alpha_0} \right\} e^{-2\alpha_0 t}, \quad \forall t > 0 \quad (83)$$

The sliding surface \bar{S} and the approximation errors of RBFNN (\tilde{W}_a , \tilde{W}_b , and \tilde{W}_c) are uniformly ultimately bounded.

Table A1: VSWT System Parameters.

Parameters	Values	Parameters	Values
ρ = Air density	1.225 kg/m^3	D_s = Shaft damping coefficient	8.3478×10^7
$P_{e, \text{nom}}$ = Nominal power	$5 \times 10^6 \text{ W}$	R = Rotor radius	63 m
N_g = Gear ratio	97	H = Height of tower	90 m
$\omega_{r, \text{nom}}$ = Nominal angular velocities of rotor	1.26 rad/sec	M_t = Mass constant of tower	$4.2278 \times 10^5 \text{ kg}$
$\omega_{g, \text{nom}}$ = Nominal angular velocities of generator	122.91 rad/sec	K_t = Spring constant of tower	$1.6547 \times 10^6 \text{ Nm/rad}$
$\omega_{g, \text{min}}$ = Minimum angular velocities of generator	70.16 rad/sec	D_t = Damping constant of tower	2.0213×10^3
J_r = Rotor inertia	$5.9154 \times 10^7 \text{ kgm}^2$	ω_n = Natural frequency of the actuator	0.88 rad/sec
J_g = Generator inertia	500 kgm^2	ζ = Damping of pitch actuator	0.9
K_s = Spring constant	$8.7354 \times 10^8 \text{ Nm/rad}$	τ_T = Time constant	0.1 sec

REFERENCES

- Asghar, A. B. & Liu, X. 2018.** Adaptive neuro-fuzzy algorithm to estimate effective wind speed and optimal rotor speed for variable-speed wind turbine. *Neurocomputing*, **272**: 495-504.
- Byrnes, C. I. & Isidori, A. 1984.** A frequency domain philosophy for nonlinear systems, with application to stabilization and to adaptive control. 23rd IEEE Conference on Decision Control, 1: 1569–1573.
- Chang, Y. H. & Chan, W. S., 2014.** Adaptive dynamic surface control for uncertain nonlinear systems with interval type-2 fuzzy neural networks. *IEEE Transactions on Cybernetics*, **44**(2): 293-304.
- Ciccarelli, O., Corradini, M. L., Cucchieri, G., Ippoliti, G. & Orlando, G. 2012.** Sliding mode control based robust observer of aerodynamic torque for variable-speed wind turbines. 38th Annual Conference on IEEE Industrial Electronics Society (IECON), 4332-4337.
- Corradini, M. L., Ippoliti, G. & Orlando, G. 2013.** Robust control of variable-speed wind turbines based on an aerodynamic torque observer. *IEEE Transactions on Control Systems Technology*, **21**(4): 1199-1206.
- Dahbi, A., Said, N. N. & Said, M. S. N. 2016.** A novel combined MPPT-pitch angle control for wide range variable speed wind turbine based on neural network. *International Journal of Hydrogen Energy*, **41**(22): 9427-9442.
- De Wit, C. C., Olsson, H., Astrom, K. J. & Lischinsky, P. 1995.** A new model for control of systems with friction. *IEEE Transactions on automatic control*, **40**(3): 419-425.
- Do, H. T., Dang, T. D., Truong, H. V. A. & Ahn, K. K. 2018.** Maximum Power Point Tracking and Output Power Control on Pressure Coupling Wind Energy Conversion System. *IEEE Transactions On Industrial Electronics*, **65**(2): 1316-1324.
- Do, T. D. 2017.** Disturbance observer-based fuzzy SMC of WECSs without wind speed measurement. *IEEE Access*, **5**: 147-155.
- Douak, M., Aouachria, Z., Rabehi, R. & Allam, N. 2018.** Wind energy systems: Analysis of the self-starting physics of vertical axis wind turbine. *Renewable and Sustainable Energy Reviews*, **81**: 1602-1610.
- Engleitner, R., Nied, A., Cavalca, M. S. M. & Costa, J. P. D. 2018.** Dynamic Analysis of Small Wind Turbines Frequency Support Capability in a Low-Power Wind-Diesel Microgrid. *IEEE Transactions on Industry Applications*, **54**(1): 102-111.
- Errami, Y., Ouassaid, M. & Maaroufi, M. 2015.** A performance comparison of a nonlinear and a linear control for grid connected PMSG wind energy conversion system. *Electrical Power and Energy Systems*, **68**: 180-194.
- Fan, Y., Mu, A. & Ma, T. 2016.** Modeling and control of a hybrid wind-tidal turbine with hydraulic accumulator. *Energy*, **112**: 188-199.

- Galeazzi, R., Gryning, M. P. & Blanke, M. 2013. Observer backstepping control for variable speed wind turbine. IEEE American Control Conference (ACC), 1036-1043.
- Henriksen, L.C., 2007. Model predictive control of a wind turbine. Master's thesis, Technical University of Denmark.
- Jafarnejadsani, H., Pieper, J. & Ehlers, J. 2013. Adaptive control of a variable-speed variable-pitch wind turbine using radial-basis function neural network. IEEE transactions on control systems technology, **21**(6): 2264-2272.
- Jain, A., Schilbach, G., Fagiano, L. & Morari, M. 2015. On the design and tuning of linear model predictive control for wind turbines. Renewable Energy, **80**: 664-673.
- Kamal, E., Aitouche, A., Ghorbani, R. & Bayart, M. 2013. Robust nonlinear control of wind energy conversion systems. International Journal of Electrical Power & Energy Systems, **44**(1): 202-209.
- Laghrouche, S., Ahmed, F. S. & Mehmood, A. 2014. Pressure and friction observer-based backstepping control for a VGT pneumatic actuator. IEEE Transactions on Control Systems Technology, **22**(2): 456-467.
- Lewis, F.L., Jagannathan, S. & Yesildirek, A., 1998. Neural network control of robot manipulators and nonlinear systems. Taylor and Francis, CRC Press, Bristol, PA, USA.
- Majd, V. J. & Mobayen, S. 2015. An ISM-based CNF tracking controller design for uncertain MIMO linear systems with multiple time-delays and external disturbances. Nonlinear Dynamics, **80**(1-2): 591-613.
- Merabet, A., Rajasekaran, V., McMullin, A., Ibrahim, H., Beguenane, R. & Thongam, J. S. 2013. Nonlinear model predictive controller with state observer for speed sensorless induction generator-wind turbine systems. Proceedings of the Institution of Mechanical Engineers, Part I: Journal of Systems and Control Engineering, **227**(2): 198-213.
- Merida, J. O., Davila, J. A. & Aguilar, L. T. 2012. Robust quasi-continuous sliding-mode control of a variable-speed wind turbine. 9th IEEE Conference on Computing Science and Automatic Control (CCE), 1-6.
- Merida, J., Aguilar, L. T. & Davila, J. 2014. Analysis and synthesis of sliding mode control for large scale variable speed wind turbine for power optimization. Renewable Energy, **71**: 715-728.
- Mobayen, S. & Baleanu, D. 2016. Stability analysis and controller design for the performance improvement of disturbed nonlinear systems using adaptive global sliding mode control approach. Nonlinear Dynamics, **83**(3): 1557-1565.
- Mobayen, S. (2015). Design of a robust tracker and disturbance attenuator for uncertain systems with time delays. Complexity, **21**(1): 340-348.
- Mobayen, S. 2016. A novel global sliding mode control based on exponential reaching law for a class of underactuated systems with external disturbances. Journal of Computational and Nonlinear Dynamics, **11**(2): 021011, 1-9.
- Moradi, H. & Vossoughi, G. 2015. Robust control of the variable speed wind turbines in the presence of uncertainties: A comparison between H_∞ and PID controllers. Energy, **90**: 1508-1521.
- Njiri, J. G. & Soffker, D. 2016. State-of-the-art in wind turbine control: Trends and challenges. Renewable and Sustainable Energy Reviews, **60**: 377-393.
- Patel, M. & Pratap, B. 2018. Design of an adaptive neuro-observerbased feedback controller for high-speed trains with parametric uncertainties. Proceedings of the Institution of Mechanical Engineers, Part F: Journal of Rail and Rapid Transit, Article Available Online.
- Pratap, B. & Purwar, S. 2013. Real-time implementation of state observers for twin rotor MIMO system: an experimental evaluation. International Journal of Modelling, Identification and Control, **19**(1): 98-110.
- Pratap, B. & Purwar, S. 2014. Real Time Implementation of Neuro Adaptive Observer Based Robust Backstepping Controller for Twin Rotor MIMO System. Journal of Control, Automation and Electrical Systems, **25**(2): 137-150.
- Pratap, B. & Purwar, S. 2018a. Real-Time Implementation of Nonlinear State and Disturbance Observer Based Controller for Twin Rotor Control System. International Journal of Automation and Control, Article in Press.
- Pratap, B., Singh, N. & Kumar, V. 2018b. Robust Control of Variable Speed Wind Turbine Using Quasi-Sliding Mode Approach. 6th International Conference on Smart Computing and Communications. Procedia Computer Science, Kurukshetra, India, **125**: 398-404.
- Ren, Y., Li, L., Brindley, J. & Jiang, L. 2016. Nonlinear PI control for variable pitch wind turbine. Control Engineering Practice, **50**: 84-94.
- Rezaei, M. M., Behzad, M., Haddadpour, H. & Moradi, H. 2015. Development of a reduced order model for nonlinear analysis of the wind turbine blade dynamics. Renewable Energy, **76**: 264-282.

- Seker, M., Zergeroglu, E. & Tatlicioglu, E. 2015.** Non-linear control of variable-speed wind turbines with permanent magnet synchronous generators: a robust Backstepping approach. *International Journal of Systems Science*, **47**(2): 420-432.
- Shaik, F. A., Purwar, S. & Pratap, B. 2011.** Real-time implementation of Chebyshev neural network observer for twin rotor control system. *Expert Systems with Applications*, **38**(10): 13043-13049.
- Shtessel, Y., Edwards, C., Fridman, L. & Levant, A. 2014.** Sliding mode control and observation. Springer, New York.
- Singh, N., Pratap, B. & Swarup, A. 2016.** Design of Robust Control for Wind Turbine Using Quantitative Feedback Theory. 4th IFAC Conference on Advances in Control and Optimization of Dynamical Systems. Tiruchirappalli, India, **49**(1): 718-723.
- Singh, N., Pratap, B. & Swarup, A. 2017.** Discrete-Time Robust Control of Variable Speed Wind Turbine Using Quantitative Feedback Theory. 14th IEEE India Council International Conference. Roorkee, India.
- Singh, N., Pratap, B. & Swarup, A. 2018.** Robust control design of variable speed wind turbine using quantitative feedback theory. *Proceedings of the Institution of Mechanical Engineers, Part A: Journal of Power and Energy*, **232**(6): 691-705.
- Slotine, J.J.E. & Li, W. 1991.** Applied nonlinear control, Prentice Hall, New Jersey.
- Song, D., Yang, J., Dong, M. & Joo, Y. H. 2017.** Model predictive control with finite control set for variable-speed wind turbines. *Energy*, **126**: 564-572.
- Soued, S., Ebrahim, M. A., Ramadan, H. S. & Becherif, M. 2017.** Optimal blade pitch control for enhancing the dynamic performance of wind power plants via metaheuristic optimisers. *IET Electric Power Applications*, **11**(8): 1432-1440.
- Soufi, Y., Kahla, S. & Bechouat, M. 2016.** Feedback linearization control based particle swarm optimization for maximum power point tracking of wind turbine equipped by PMSG connected to the grid. *International Journal of Hydrogen Energy*, **41**: 20950–20955.
- Stevanovic, N., Green, P. L., Worden, K. & Kirkegaard, P. H. 2016.** Friction estimation in wind turbine blade bearings. *Structural Control and Health Monitoring*, **23**(1): 103-122.
- Thomsen, S.C., 2006.** Nonlinear Control of a Wind Turbine. Master's thesis, Technical University of Denmark.
- Toulabi, M., Dobakhshari, A. S. & Ranjbar, A. M. 2017.** An adaptive feedback linearization approach to inertial frequency response of wind turbines. *IEEE Transactions on Sustainable Energy*, **8**(3): 916-926.
- Viveiros, C., Melicio, R., Igreja, J. M. & Mendes, V. M. F. 2015.** Supervisory control of a variable speed wind turbine with doubly fed induction generator. *Energy Reports*, **1**: 89-95.
- Xin, W., Wanli, Z., Bin, Q. & Pengcheng, L. 2014.** Sliding mode control of pitch angle for direct driven PM wind turbine. 26th Chinese IEEE Conference on Control and Decision (CCDC), 2447-2452.
- Yang, S., Guo, L., Qi, L., Chang, L. & Zhang, X. 2015.** A parameter-robust sliding mode observer for speed sensorless torque control of PMSG in wind power generation system. 28th IEEE Canadian Conference on Electrical and Computer Engineering (CCECE), 1083-1087.
- Zhang, L., Chunliang, E., Li, H. & Xu, H. 2009.** A new pitch control strategy for wind turbines base on quasi-sliding mode control. *IEEE Conference on Sustainable Power Generation and Supply (SUPERGEN)*, 1-4.
- Zhang, Z. Z., Zou, J. X., Zheng, G. & Xu, H. B. 2012a.** Observer-based backstepping control of the half-direct permanent magnet wind power generation system. *Proceedings of the Institution of Mechanical Engineers, Part I: Journal of Systems and Control Engineering*, **226**(4): 441-450.
- Zhang, Z., Zhao, Y., Qiao, W. & Qu, L. 2012b.** A space-vector modulated sensorless direct-torque control for direct-drive PMSG wind turbines. *IEEE Industry Applications Society Annual Meeting (IAS)*, 1-7.
- Zhou, Y., Chen, M. & Jiang, C. 2015.** Robust tracking control of uncertain MIMO nonlinear systems with application to UAVs. *IEEE/CAA Journal of Automatica Sinica*, **2**(1): 25-32.
- Zu, H., Zhang, G. & Fei, S. et al. 2012.** Robust control for a direct-driven permanent magnetic synchronous generator without mechanical sensors based on model reference adaptive Backstepping control method. *Proceedings of the Institution of Mechanical Engineers, Part I: Journal of Systems and Control Engineering*, **226**(8): 1130-1141.

Submitted: 10/03/2018

Revised: 13/04/2018

Accepted: 30/04/2018

تصميم وحدة تحكم تكيفية مرتكزة على مراقب لا خطي قوي لتوربينات الرياح متغيرة السرعة

*نافديب سينج، *بهانو براتاب و *أخيليش سواروب
 *كلية الطاقة المتجددة والكفاءة، المعهد الوطني للتكنولوجيا، كوروكشتر، الهند
 **قسم الهندسة الكهربائية، المعهد الوطني للتكنولوجيا، كوروشيترا، الهند

الخلاصة

يقترح هذا البحث وحدة تحكم تكيفية قائمة على مراقب لا خطي قوي لتوربين الرياح ثلاثي الشفرات ذي السرعات المتغيرة (VSWT). ونتيجة لعدم انتظام سرعة الرياح، يعتبر النموذج الديناميكي الهوائي لـ VSWT لا خطي وغير مؤكد بدرجة عالية. ونظراً لأن سرعة الدوار هي الحالة الوحيدة القابلة للقياس، فقد تم تصميم مراقب الوضع المنزلق (SMO) لتقدير الحالات غير القابلة للقياس. تم كذلك استخدام مراقب لا خطي للاحتكاك والضوضاء (NFDO) للتعامل مع الاضطرابات الخارجية والآثار الاحتكاكية عبر عمود الدوار والمولد في منظومة VSWT. وعلى أساس أجهزة المراقبة المقترحة (SMO و NFDO)، تم تطوير مسيطر للتغذية المرتدة للخروج لـ VSWT باستخدام تقنية التحكم في الوضع شبه المنزلق. تم تصميم المسيطر المقترح القائم على المراقب لالتقاط أقصى قدر من الطاقة المتاحة من الرياح في ظل أوجه عدم اليقين. تم إثبات استقرار الحلقة المغلقة للمسيطر المقترح باستخدام خوارزمية *design Lyapunov-like*. أجريت دراسات المحاكاة التفصيلية لتوضيح الأداء القوي لنظام المراقبة المقترح. وأخيراً، تم إجراء تحليل مقارن للمسيطر التكيفي المقترح مع وحدات تحكم مختلفة لضمان أداء تعقب قوي مع تأثير تذبذب منخفض، وأخطاء تتبع أقل وجهود تحكم محددة.